

DOI: [10.29026/oea.2022.210029](https://doi.org/10.29026/oea.2022.210029)

# Piezoresistive design for electronic skin: from fundamental to emerging applications

Fang Zhong<sup>1</sup>, Wei Hu<sup>1</sup>, Peining Zhu<sup>2</sup>, Han Wang<sup>3,4</sup>, Chao Ma<sup>1</sup>, Nan Lin<sup>1</sup>  
and Zuyong Wang<sup>1\*</sup>

There is growing recognition that the developments in piezoresistive devices from personal healthcare to artificial intelligence, will emerge as *de novo* translational success in electronic skin. Here, we review the updates with regard to piezoresistive sensors including basic fundamentals, design and fabrication, and device performance. We also discuss the prosperous advances in piezoresistive sensor application, which offer perspectives for future electronic skin.

**Keywords:** electronic skin; piezoresistive sensor; biocompatibility

Zhong F, Hu W, Zhu PN, Wang H, Ma C et al. Piezoresistive design for electronic skin: from fundamental to emerging applications. *Opto-Electron Adv* 5, 210029 (2022).

## Introduction

Skin is the largest organ that not only protects our bodies from the environment, but also as a system senses and converts external stimuli into physiological signals<sup>1</sup>. The concept of electronic skin (e-skin) that represents a device to mimic natural skin, is developing explosively<sup>2-4</sup> and in order to be user friendly, it aims to rebuild the skin's sensing response to the vital characteristic, e.g. strain, pressure, temperature, moisture, and body fluid composition, and offer enough flexible, durable and self-healing properties<sup>5-9</sup>. Historically, in 1985 General Electric developed the first skin-like electronic device to offer the sensing capability for robotic arms (Fig. 1(a))<sup>10</sup>. This progress initiates the appearance of e-skin in public vision and causes great research enthusiasm with significant developments, e.g. capabilities of shear force measurement<sup>11</sup>, spatial tactile mapping<sup>12</sup>, connection between e-skin and live neuron<sup>13</sup>, bioinspired and large-area man-

ufacturing<sup>14-16</sup>, and self-healing property<sup>17</sup>. Meanwhile, the achievement of conductive composite makes e-skin possible to integrate flexibility with high sensitivity. For example, Lou et al.<sup>18</sup> designed a composite for e-skin, by incorporation of reduced graphene oxide (rGO) in a flexible polymer matrix. Park et al.<sup>19</sup> reported a ferroelectric e-skin with a complex three-dimensional (3D) microstructure, which could detect and amplify signals from temperature, pressure, and vibration change simultaneously. Latest developments on the sensitive response to sound, magnetic field, and ultraviolet light are expected to make e-skin be functional beyond natural skin<sup>20,21</sup>. With real-time monitoring, timely feedback, wireless sensing, and ease to carry, there is a strong expectation that e-skin will display more advanced and convenient features than existing health-monitoring devices. Future e-skin shall be able to sense external stimuli and in turn crosstalk with the human neural network<sup>10,22</sup>.

<sup>1</sup>College of Materials Science and Engineering, School of Physics and Electronics, Hunan University, Changsha 410072, China; <sup>2</sup>Hunan Aerospace Magnet & Magneto Co., LTD, Changsha 410200, China; <sup>3</sup>State Key Laboratory of Precision Electronic Manufacturing Technology and Equipment, Guangzhou 510006, China; <sup>4</sup>Jihua Laboratory, Foshan 528251, China.

\*Correspondence: ZY Wang, Email: wangzy@hnu.edu.cn

Received: 1 May 2021; Accepted: 24 July 2021; Published online: 25 August 2022; Available Online: 20 May 2022



**Open Access** This article is licensed under a Creative Commons Attribution 4.0 International License.

To view a copy of this license, visit <http://creativecommons.org/licenses/by/4.0/>.

© The Author(s) 2022. Published by Institute of Optics and Electronics, Chinese Academy of Sciences.

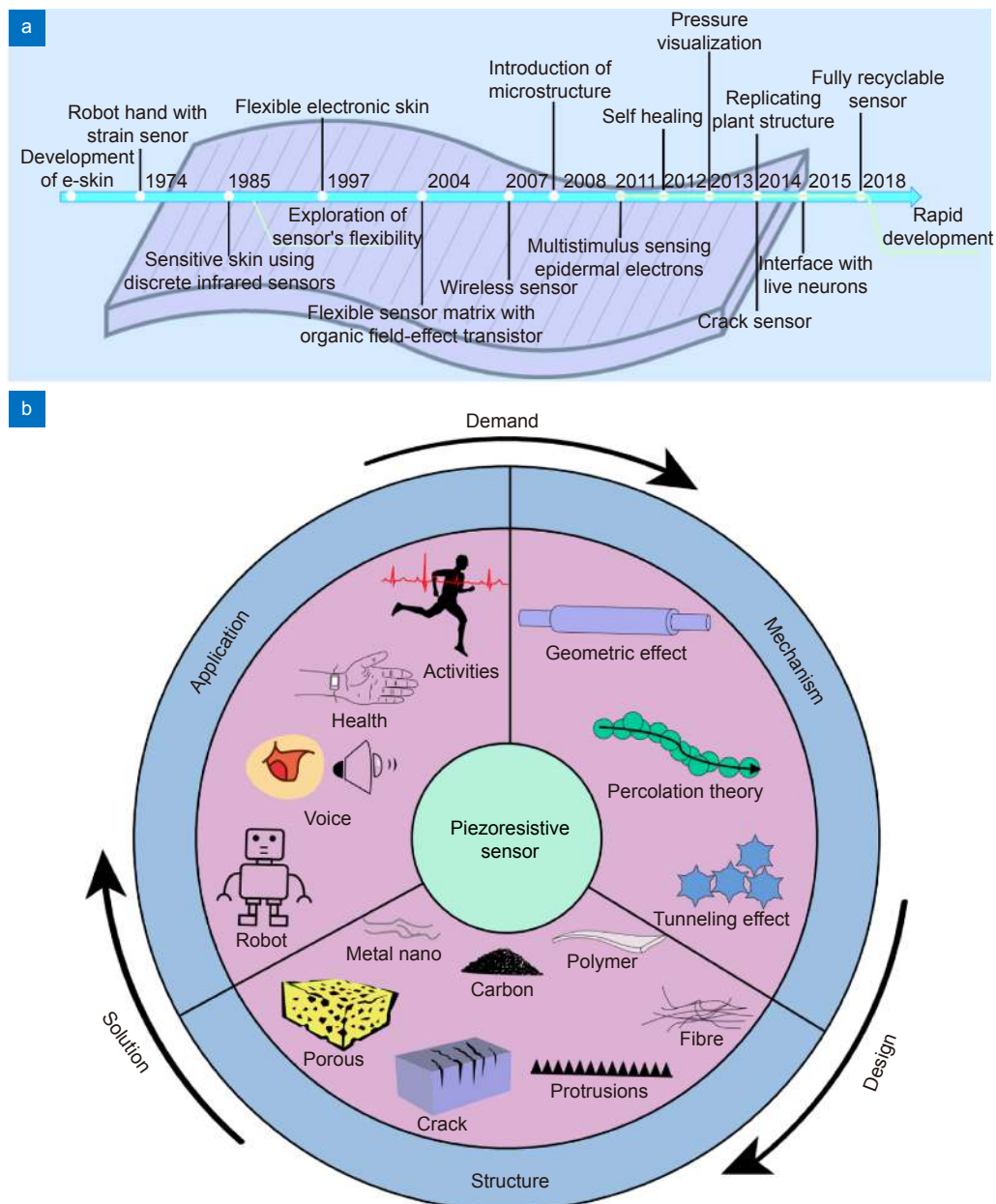


**Fig. 1 | Piezoresistive designs for engineering electronic skin. (a)** Developmental history of flexible skin-like electronics (e.g. milestones in the shear force measurement, large-area manufacturing, spatial mapping, bioinspired manufacturing, interconnection between e-skin and live neurons, and self-healing capability)<sup>10–17</sup>. **(b)** Scheme illustrating the design and applications of piezoresistive sensors.

The different receptors of natural skin confer rich sensations<sup>23</sup>. A tactile sensor that mimics response to skin touch demonstrates exciting potential, for the e-skin application in wearable health-monitoring, advanced robotics, and artificial intelligence. For example, e-skin based on a tactile sensor could sense complex mechanical parameters, e.g. strength, position, and time sequence of the applied force<sup>24</sup>. Differently, e-skin based on temperature and chemical sensors could respond to thermal variation<sup>25,26</sup>, and biofluid<sup>5</sup>, respectively. Presently, the working principle of a tactile sensor can be capacitive,

piezoelectric and piezoresistive, which accounts for the sensor with a micro-level resolution to mechanical force whilst reducing manufacturing cost and complexity<sup>24</sup>. However, a capacitive sensor may associate with vulnerable sensitivity and parasitic capacitance that give the unstable performance of e-skin<sup>27,28</sup>. A piezoelectric sensor can have the high sensitivity for precise dynamic stimulus detection, except static mechanics or the one at a magnitude beyond nanoscale<sup>29</sup>. In contrast, the piezoresistive sensor enables the detection of both static and dynamic stimulus at high sensitivity, fast response, a large

sensing range and better low frequency response, and is advanced in simple assembling and low-cost fabrication<sup>30</sup>.

Current versatile designs of piezoresistive sensor find extensive research for e-skin development<sup>31</sup>, leading to the emergence of a wide range of application, including muscle contraction measurement<sup>31</sup>, gait monitoring<sup>32</sup>, voice recognition<sup>33</sup>, robotic control<sup>34</sup> and human-machine interaction<sup>35</sup>. On the other hand, existing challenging issues toward transformation remain not solved yet and waiting for a *de novo* solution<sup>36</sup>. Here, we present a systemic review on the updated status of the piezoresistive sensor (Fig. 1(b)). We attempt to uncover the fundamentals, structure design, manufacturing, and performance for piezoresistive innovation. We also discuss the healthcare relevance of piezoresistive sensor-based e-skin and propose future perspectives for this field. This review has significant insights into designing advanced piezoresistive sensors for future e-skin.

## Mechanisms of piezoresistive materials

By definition, the piezoresistive effect represents the change of electrical resistance under mechanical stress and strain<sup>37</sup>. It can be quantified by Gauge Factor (GF), which is equal to a ratio of the relative resistance change to applied mechanical deformation:  $GF = \frac{\Delta R/R}{\varepsilon} = \frac{\Delta \rho/\rho}{\varepsilon} + (1 + 2\gamma)$ , where  $R$ ,  $\rho$  and  $\gamma$  are the material's resistance, resistivity and Poisson's ratio, respectively<sup>38</sup>. The GF of most metallic materials is between 1.6 and 2, and under mechanical stimuli, it often varies by geometric change<sup>39</sup>. Differently, upon receiving mechanical stimuli, semiconductors can change their density and mobility of charge carriers, leading to a variation to the material's GF<sup>40</sup>.

### Piezoresistive effects from metals and conductive inorganic non-metallic materials

#### Metallic materials

The electrical resistance of a metal depends on its dimension and resistivity. When subjected to mechanical stimuli, the metal follows Poisson's ratio to adjust its dimensions in length and cross-sectional area whilst giving less change to its resistivity (Fig. 2(a)). As such, the variation in metallic resistance is a function of geometric change, which forms the fundamentals of the piezoresistive effect<sup>41</sup>. For example, a metallic bent strip at a thickness of few microns has application in different strain gauges<sup>42</sup>.

Such a traditional piezoresistive sensor is advanced in low-cost manufacture and high sensitivity, but remains with challenging issues when integrated into a flexible e-skin and applied for the detection in different directions<sup>43</sup>. These limitations related to metallic material could be resolved by manufacturing advances. For instance, wafer-scale microfabrication can allow for embedding metal gauge on polymer chip, thereby enabling in-situ stain monitoring<sup>44</sup> and pressure sensing<sup>45</sup>.

Further extension of piezoresistive fundamental by integration between metal and polymer, makes the wider and more convenient application of metal for the flexible device. For example, nanometal as the conductive filler can be dopped into a flexible polymer matrix and generates a piezoresistive effect by establishing percolating networks (Refer to 'Nonconductive polymers'). Different from the direct blending, Ferreira et al.<sup>38</sup> reported deposition of the nanostructured zigzag-like ZnO/Ag thin film on polyethylene terephthalate substrate and assembled them into a flexible and stretchable piezoresistive strain sensor. Alternatively, Peng et al.<sup>46</sup> developed a flexible foam for piezoresistive sensor construction, by a liquid metal coating during polymerisation, and obtained a super electrical conductivity, high elasticity, and phenomenal mechanical stability (Fig. 3(a)).

#### Conductive inorganic non-metallic materials

Due to the excellent comprehensive properties, carbon materials are becoming one of the most popular and competitive conductive fillers for piezoresistive sensor and e-skin development. Similar to the metallic nanomaterials, nanoscale carbon black, fibre, and tube could form piezoresistive composite for e-skin application, by direct blending with different polymers<sup>49</sup>. Shajari et al.<sup>50</sup> developed an ultralow percolated thin film comprising of polar fluoroelastomer and carbon nanotube (Fig. 3(b)). This nanocomposite film was fabricated by an optimised internal melt-mixing process followed with common compression molding. The film was suggested to have a double-percolating electrical network that could offer simultaneous superb sensitivity for both low and high strain values and achieve a high GF of  $1.3 \times 10^5$  at much lower filler content (2 phr). Based on the composite comprising of graphite filler and polyurethane elastomer, He et al.<sup>51</sup> reported a flexible piezoresistive sensor that showed high sensitivity, high reliability, and low-cost fabrication. The filler modification and concentration were found to affect the electrical conductivity of the

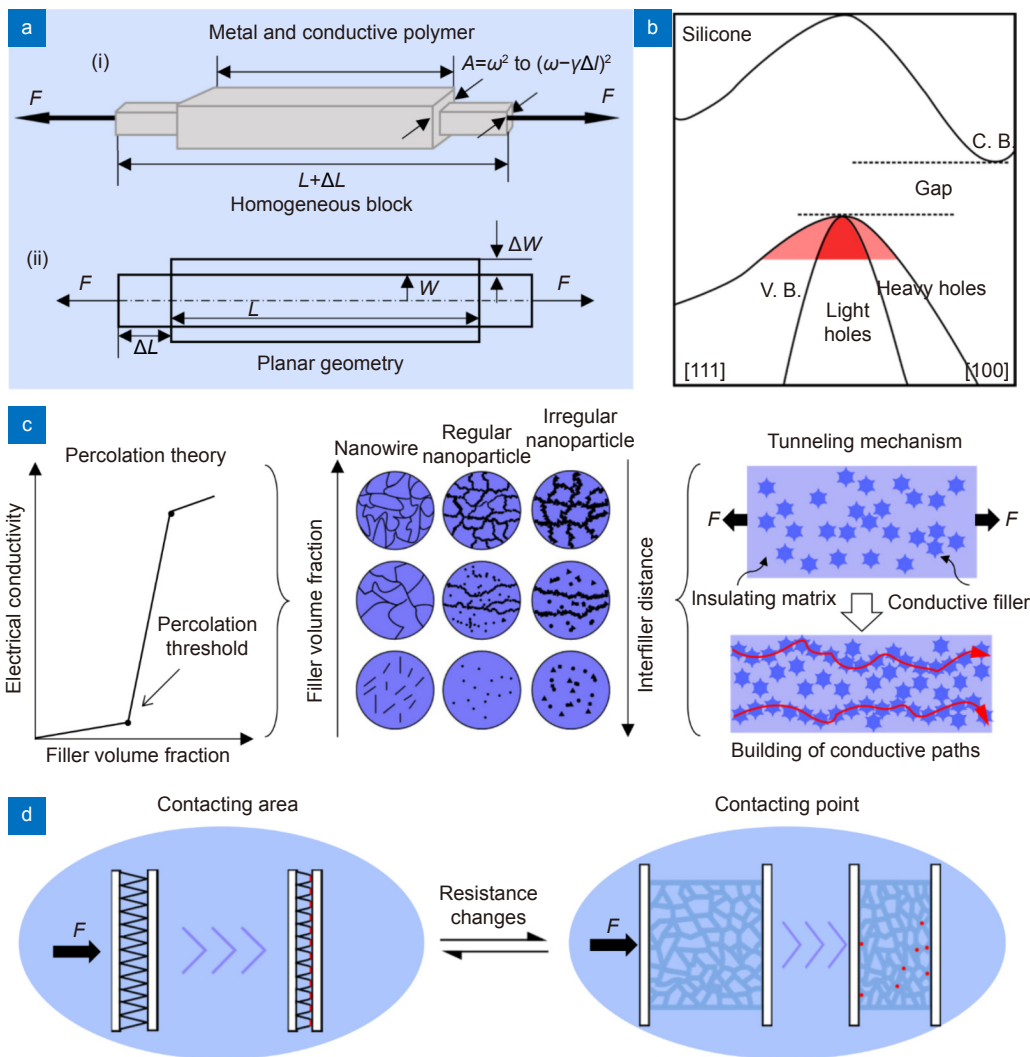


**Fig. 2 | Principles of piezoresistive effect.** (a) Piezoresistance based on the geometric changes of metals and conducting polymers. i and ii represent the block and planar material geometries, respectively<sup>41,47</sup>. (b) Piezoresistance of semiconductor. Scheme illustrating the changes of charge carrier and energy band upon traction along the [111] direction in p-Si<sup>47</sup>. (c) Piezoresistance of composite materials based on the changes of conducting filler concentration and inter-filler distance<sup>48</sup>. (d) Structural piezoresistance based on the contact area and point changes of conducting architecture. Figure reproduced with permission from: (b) ref.<sup>47</sup>, Elsevier.

composite films, which showed a percolation threshold at 28.03 wt% of modified-graphite and a piezoresistive sensitivity of 0.274 kPa<sup>-1</sup> at 30 wt% of modified-graphite under uniaxial compression (Fig. 3(c))<sup>51</sup>. This piezoresistance is believed due to the effect of coupling mechanical deformation and electrical property of a percolating carbon network established within the polymeric matrix<sup>51</sup>. Taken carbon nanotube for example, there exist two types of resistances that account for the strain-sensing mechanism, including an intrinsic resistance of carbon nanotube and an intertube resistance. The latter occurs when the gap between adjacent carbon nanotubes is small enough to induce a conductive path at the external electronic field both due to a “tunneling” as well

as a “hopping” mechanism. In addition to the direct blending, carbon materials could also be fabricated into a piezoresistive sponge, which is capable of overcoming the problems related to conductive nanomaterial coating, e.g. fragile, easy to peel off, and material aggregation<sup>52</sup>.

### Piezoresistive effects from semiconductors

Semiconductive materials such as silicon, polysilicon, and silicon carbide, have inherent piezoresistive property, and due to less correlation to geometric change, their piezoresistivity is distinct from metallic materials. The existing theories are based on the modifications to the energy band structure (not only the band gap but also the band warping and splitting). In this paradigm,

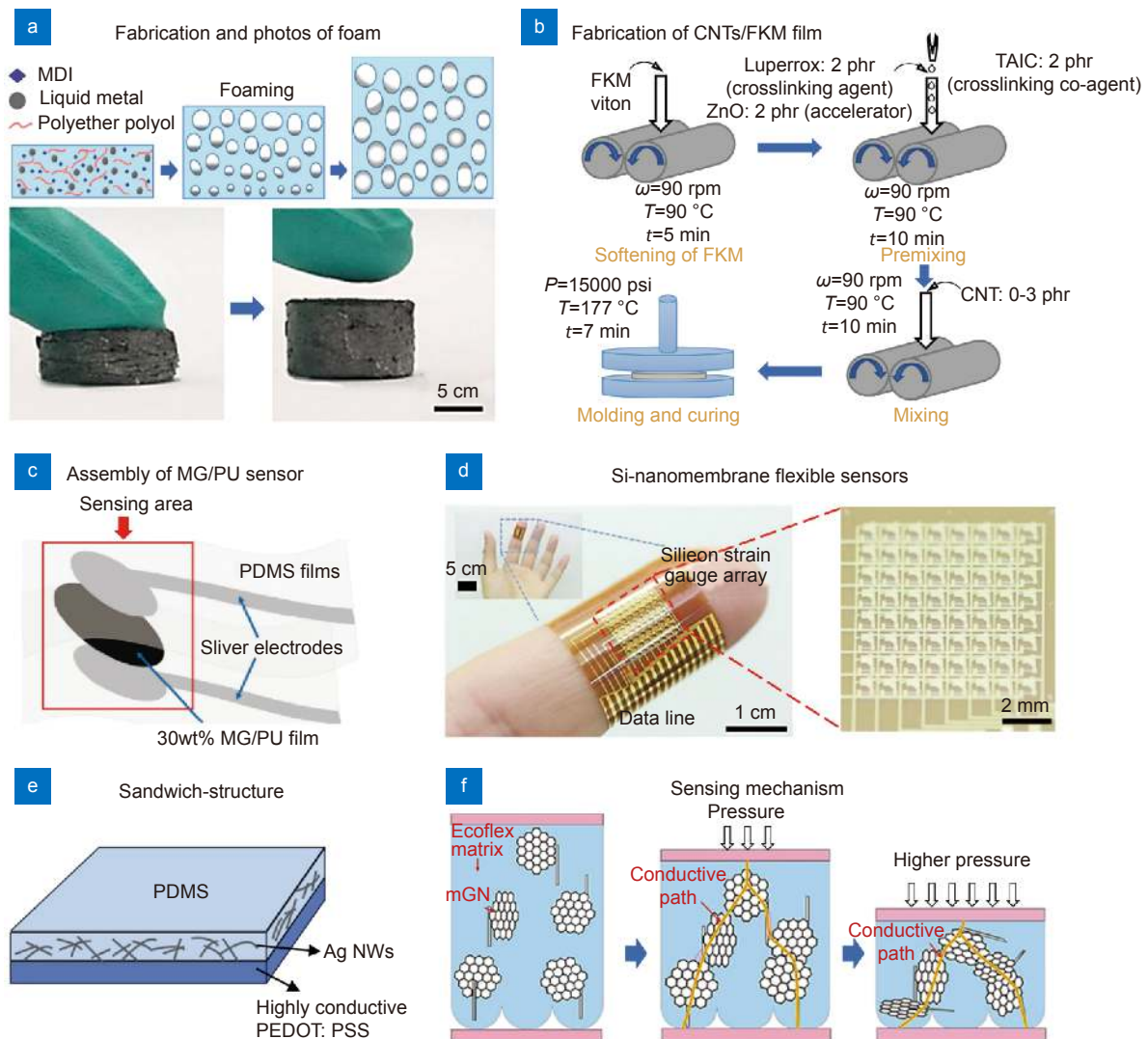


**Fig. 3 | Development of piezoresistive sensors based on various materials.** (a) Fabrication scheme and optical images of a hybrid metallic foam<sup>46</sup>. (b) Schematic illustrating the fabrication of CNTs/FKM nanocomposite<sup>50</sup>. FKM, fluoroelastomer; CNTs, carbon nanotubes; and TAIC, 1,3,5-triallyl-1,3,5-triazine-2,4,6 (1H,3H,5H)-trione. (c) Scheme illustrating the assembly of a MG/PU piezoresistive sensor<sup>51</sup>. MG, modified-graphite; PU, polyurethane; and PDMS, polydimethylsiloxane. (d) A flexible tactile sensor assembled from the 8x8 array of Si-strain gauges and the Si thin film transistors<sup>64</sup>. (e) Scheme illustrating the sandwich-structure of a PEDOT:PSS/Ag NW/PDMS component film<sup>74</sup>. PEDOT:PSS, poly(3,4-ethylenedioxythiophene):poly(styrenesulfonate); and Ag NWs: Ag nanowires. (f) mGN fillers form new conducting paths under pressure<sup>80</sup>. mGN, magnetic reduced graphene oxide@nickel nanowire. Figure reproduced with permission from: (a) ref.<sup>46</sup>, (f) ref.<sup>80</sup>, American Chemical Society; (c) ref.<sup>51</sup>, under a Creative Commons Attribution 4.0 International License; (d) ref.<sup>64</sup>, AIP Publishing.

the strain in a crystalline solid can change the lattice constants and reduce crystal symmetry, leading to the significant shifts in energy band edges<sup>53</sup>. This bandgap shift and the change in electrons mass under strain lead to the change in conductivity and carrier mobility. In another word, the effect of applied force is to change the number and mobility of charge carriers within a material, thus causing large changes in resistivity (Fig. 2(b))<sup>40,42,47</sup>. This results in the piezoresistive semiconductor having very high sensitivity and better low frequency response than its piezoelectric effect. Taken silicon for example, its res-

istance change after the force applied can be expressed as  $\frac{\Delta R}{R} = \frac{\Delta \rho}{\rho} = \pi_l \sigma_l + \pi_t \sigma_t$ , where  $\pi_l$  and  $\pi_t$  are piezoresistive coefficients along and across force directions, respectively, and  $\sigma_l$  and  $\sigma_t$  represent the longitudinal and transverse stresses, respectively<sup>47</sup>.

Several factors are reported to influence GF and piezoresistance coefficient strongly including the type and level of doping material, crystallographic direction and material's elasticity and dimension: (1) Doping type - Under external stress, the n-/p-type piezoresistors have

opposite trends in resistance change and different direction-dependent magnitudes. For the maximum sensitivity, n-type silicon piezoresistor must be aligned along [100] direction, and p-type piezoresistor along [110] direction<sup>54</sup>. N-type silicon shows a negative GF of about -135 and the p-type silicon a positive GF up to 175<sup>47</sup>; (2) Doping level - In the highly-doped silicon piezoresistor, the percentage of carriers moving toward the lower energy levels is smaller than that at a low-impurity concentration. This leads to the low-doped piezoresistor having a high GF<sup>47</sup>; (3) Crystallographic direction - Most theoretical models have the crystal orientation dependence of band structure, electron energy and the effective masses of carriers. In n-type silicon, the average mobility of carriers increases in the direction of tension (longitudinal effect) and declines transverse to that direction (transverse effect)<sup>41</sup>; (4) Material's elasticity - The semiconductors such as silicon, germanium and gallium arsenide have typically elastic body. The elasticity influences what degrees of the material's deformation to given stress and in turn determines the number and mobility changes of charge carriers; (5) Scale of materials - In semiconductors, the quantum confinement effects exist when the device is sufficiently thin and have important implications for that material's energy band structure. Piezoresistance coefficient can be increased with the decrease in the scale of material. For example, the carbon nanotube can have a GF of ~2900, and the silicon nanowire has a piezoresistance coefficient reaching up to  $-3550 \times 10^{-11}/\text{Pa}$  (Bulk silicon,  $-94 \times 10^{-11}/\text{Pa}$ )<sup>53</sup>. The optimisation of these factors accounts for high sensitivity and repeatable output for the semiconductor-based piezoresistive sensors<sup>54</sup>. Based on polysilicon, Wee et al.<sup>55</sup> reported a piezoresistive micro-cantilever beam that could detect the labeled disease marker. Similarly, a piezoresistive strain sensor integrated with the silicon-based nanowire was demonstrated for accurate nerve-probe operation<sup>56</sup>.

Piezoresistive performance of the silicon-based semiconductor is temperature-dependent, and becomes unstable above 150 °C and deteriorated above 500 °C, which limits the application in the high-temperature harsh environment<sup>57</sup>. This is due to the intrinsic electron and hole mobilities of silicon that decrease with increased temperature, leading to raised resistance additionally<sup>58</sup>. Won et al<sup>59</sup> designed a 3D tactile sensor to enable simultaneous recording of pressure, shear force and bending strain along with temperature. Both temperat-

ure and the induced thermal expansion were thought to cause the change of resistance. As such, a careful control on the testing condition, addition of a temperature sensor and/or the use of Wheatstone bridge become necessary to offer extra temperature compensation, with the increases in complicity and processing cost<sup>60</sup>. In contrast, silicon carbide shows a high-temperature piezoresistive effect, due to its wide bandgap, high chemical inertness, and radiation resistance<sup>30,61</sup>. Based on the laser-induced silicon carbide, Nguyen et al<sup>62</sup> developed a piezoresistive pressure sensor, with high sensitivity in a wide range of working temperature (198–473 K). Silicon carbide incorporated into the structure of a porous sponge could enable a piezoresistive sensor for monitoring damage in the electromechanical microdevice at high temperatures<sup>63</sup>. However, the development of semiconductive piezoresistivity for e-skin remains challenging because of the high material rigidity and difficult-processing property. By transfer of silicon nanomembrane to a plastic substrate, Park et al.<sup>64</sup> proposed a solution for the assembly of a flexible piezoresistive sensor with excellent sensitivity (Fig. 3(d)). Differently, Gao et al.<sup>65</sup> applied a laser to write silicon carbide on elastomer substrate directly, thereby offering a more efficient method for the future development of the flexible piezoresistive sensor from a semiconductor.

### Piezoresistive effects from polymers

The polymeric material is investigated for piezoresistive application, in order to overcome the undeniable shortcomings related to metal and semiconductor, e.g. rigidity, small strain range, complex and high-cost manufacture<sup>66,67</sup>. The polymer has applicable prospects due to the advantages of a simple readout circuit, small crosstalk, and facile manufacture, and it can be conductive naturally or nonconductive incorporated with conductive composition<sup>68,69</sup>. For the composite, resistance raises from the changes in the conductive path, filler density, and filler contact area upon mechanical deformation<sup>70</sup>.

### Conductive polymers

Conductive polymers have piezoresistive properties, and their piezoresistance is controlled by geometric change similar to that of metals<sup>72</sup>. Take poly(3,4-ethylenedioxythiophene):poly(styrenesulfonate) (PEDOT:PSS) for example, the resistance increases in-phase with mechanical strain, probably due to the long separation between its conductive domains<sup>73</sup>. In contrast, the rearrangement

and combination of conductive domains could decrease its resistance out-of-phase with the applied strain. Due to these reasons, piezoresistive sensors based on conductive polymers can have effective sensing performance in a small range of mechanical deformation. As such, conductive polymer is often integrated with other materials, in order to obtain the idea piezoresistivity. For instance, to compensate the Ag nanowire-related permeation network Fan et al.<sup>74</sup> embedded PEDOT:PSS in polydimethylsiloxane (PDMS), and obtained a sandwich-structured piezoresistive sensor which had a reliable response, in both a cyclic stretching-releasing test and a continuous loading test (Fig. 3(e)). However, towards the wide applications in piezoresistive e-skin, conductive polymers still need to overcome challenging issues related to their long-term stability against high temperature, moisture, chemical reagent, and other harsh environments<sup>75</sup>.

### Nonconductive polymers

Most polymers are insulating in nature and can be engineered to conductive composite by incorporation with conductive materials, e.g. nanoscale metal, carbon, and conductive polymer. Piezoresistive effect of a conductive composite originates from the resistance change upon receiving external force, because of the mechanical deformation in a polymeric matrix, e.g. compress, stretch, and twisting, and the induced variation in filler distribution, e.g. the distance, contact, and conductive path among fillers<sup>76–78</sup>. Specifically, a percolation theory explains the conductivity of polymer composite: when the concentration of filler portion is below a percolation threshold, the composite with separated conductive fillers remains insulating, and it becomes conductive with a rapid decline in resistance when filler concentration is above the percolation threshold to build conductive path (Fig. 2(c))<sup>47</sup>. In this theory, the first conductive path is built just beyond the percolation threshold, by the formation of filler contacts and thus a percolating network<sup>48</sup>. The overall conductivity of a composite depends on various parameters, including the size, shape, distance, and distribution of conductive fillers<sup>39</sup>, while the total resistance is related to the resistance of each conductive filler and inter-filler contact resistance<sup>79</sup>.

Presently, conductive composites based on the percolation theory are widely applied for piezoresistive sensor development. The polymer composite by blending with conductive filler can meet the requirements of a piezoresistive e-skin sensor, e.g. flexibility and stretchab-

ility. In this paradigm, Wang et al.<sup>80</sup> reported a transparent, large-scale, and highly sensitive e-skin based on polymeric composite, which was comprised of Ecoflex and magnetic rGO@nickel nanowire (Fig. 3(f)). However, it should be noted that the highly conductive and flexible (or elastic) properties of the composite are often difficult to achieve simultaneously. This often endows a piezoresistive sensor from polymer composite with a high sensitivity but a narrow strain range<sup>81–83</sup>. The dispersion and uniformity of conductive fillers in the polymeric matrix may also influence the formation of the percolation path, and both properties could be improved by the effective modification on the filler surface<sup>84</sup>.

Polymer-based conductive composite can also be obtained by the coating and printing of conductive material on the microstructure surface of a nonconductive polymer directly, providing a high potential for piezoresistive application (Fig. 2(d)) (Refer to Section *Piezoresistive effects from metals and conductive inorganic non-metallic materials*).

## Piezoresistive structure designs and fabrication

Piezoresistive materials that possess inherent permeability and tunneling effect can respond directly to mechanical load; however, they alone are found with limitation to offer adequate sensitivity, a large detection range, rapid response, or hysteresis performance. This triggers *de novo* structure design and fabrication, with increasing interest to improve the sensing performance of a piezoresistive sensor. In the following sections, significant progress on these aspects are discussed, including most used fibre, micro/nano-structure, sponge, and additive manufacturing (AM) architecture.

### Surface-structured architecture

Structures that are designed in protrusive, cracking or a combined geometry, can be engineered from nano to micro sizes, and function as a piezoresistive portion for the flexible sensors in e-skin. These structures are capable of upregulating the sensitivity of a piezoresistive sensor greatly.

#### Protrusive structures

Artificial surface structures, such as dome<sup>85</sup>, pillar<sup>86</sup>, pyramid<sup>87</sup>, sphere<sup>88</sup>, and hierarchical structure<sup>89</sup>, are often employed for designing piezoresistive sensors for

improved sensitivity. By principle, the micro/nanostructure that connects to sensor electrodes can enlarge piezoresistive change by geometric variations between the electrodes and poorly contacted active material, even if a small mechanical load was applied<sup>90</sup>. Generally, the different high-precision structures are fabricated by photolithography on flexible substrates, although it does involve complex and high-cost procedures. For example, by photolithography Huang et al.<sup>91</sup> reported an ultra-high sensitivity of piezoresistive sensor successfully (Fig. 4(a)). Similarly, Bae et al.<sup>89</sup> developed a piezoresistive sensor, comprising of a hierarchical graphene/PDMS array, and demonstrated desirable linearity and high sensitivity (<13 kPa) to external pressure. The response linearity was due to a design of the hierarchical dome structures, which allowed accordingly for increases in the number and contact area of squeezed protuberances upon receiving larger pressure. In contrast, the dome without additional substructures had no linear response

to external pressure change.

On the other hand, lots of research efforts are keen to peruse for reducing manufacture complexity, in order to achieve a high fabrication efficiency, reproducibility, and low-cost procedures to improve the translational potential of piezoresistive sensors. In this paradigm, laser-assisted fabrication may offer a highly translational potential and stable controllability in engineering the structures for a piezoresistive sensor, with the easily modulated sensitivity via a precise control on structure geometry, e.g. ridge and dome at different sizes<sup>92</sup>. For example, the micro-cone structure that could enable great contact-area change even under tiny pressure and deformation was reported on both soft and hard substrates by laser fabrication to achieve high-sensitivity performance<sup>7,93</sup>. Hot embossing is another simple and cost-effective method, capable of developing large-scale surface structures with controlled parameters, e.g. height and diameter of micro-domes<sup>80</sup>. Previously, based on

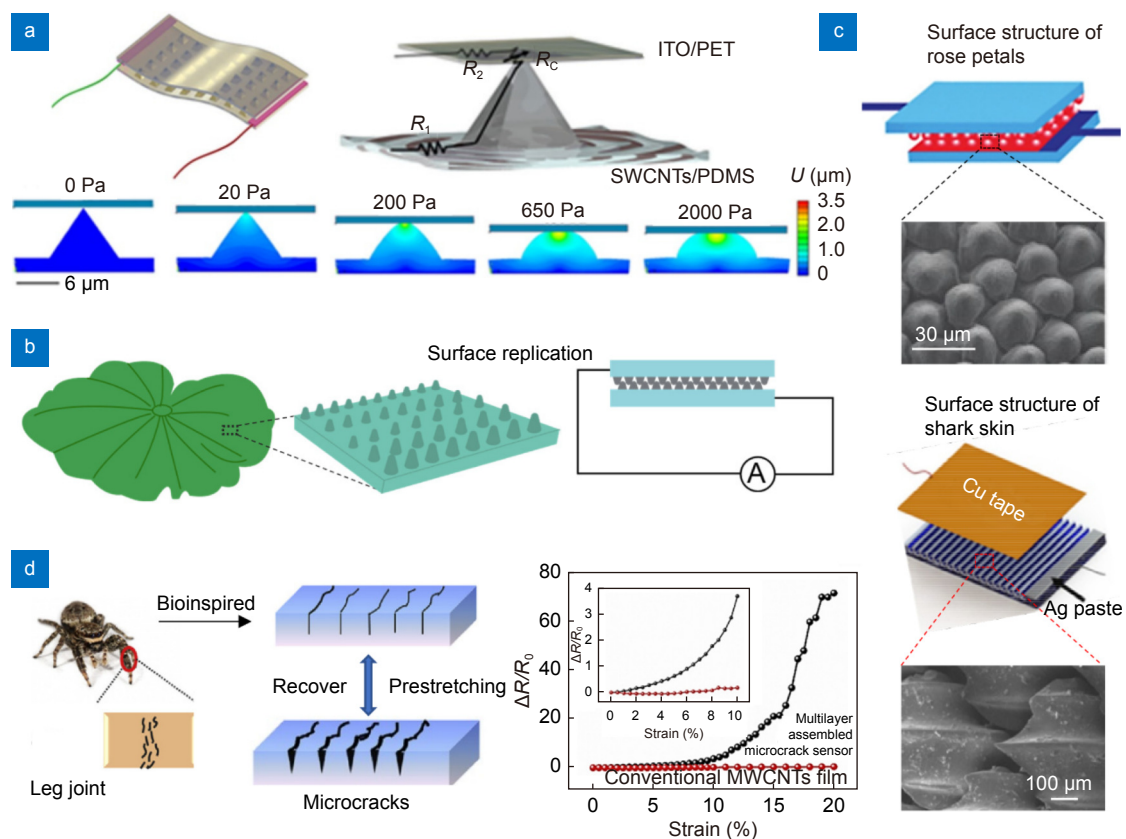


**Fig. 4 | Piezoresistive design and manufacture with singular structure.** (a) Piezoresistance of an artificial structured sensor based on contact area changes<sup>91</sup>. ITO, indium tin oxide; PET, polyethylene terephthalate; SWCNTs, single-walled carbon nanotube; PDMS, polydimethylsiloxane. (b) Scheme illustrating the lotus-leaf-inspired piezoresistive design and assembly<sup>98</sup>. (c) Scheme illustrating the rose-petal-inspired piezoresistive design and assembly<sup>99</sup> and the shark-skin-inspired piezoresistive design and assembly<sup>101</sup>. (d) Scheme illustrating the spider-leg-joint-inspired piezoresistive design with plenty of cracks<sup>102</sup>. Figure reproduced with permission from: (a) ref.<sup>91</sup>, (d) ref.<sup>102</sup>, Elsevier; (c) ref.<sup>101</sup>, Elsevier and ref.<sup>99</sup>, Royal Society of Chemistry.

CNTs/PDMS composite Park et al.<sup>94</sup> studied the performance of a piezoresistive sensor with different structures, e.g. dome, pyramid and pillar, and reported that the dome structure offered the best force sensitivities for the normal, tensile and bending stresses (Fig. 5). This was attributed to the localised stress concentration that increased the sensor's sensitivity and output range. However, a large pressure could cause the dome structure with a declined sensitivity and a short range of linear response<sup>89,95</sup>. In another study, Jia et al.<sup>96</sup> developed an even simple method by sandpaper to obtain irregular protrusions, which could also have an effective contact-area increase upon external pressure. Compared with regular structure designs, irregular pattern replication from sandpapers could serve as hierarchical microarchitectural and form additional conduction paths, to generate excellent piezoresistance with a broader sensing range and higher sensitivity.

In addition to the numerous designs of artificial structure, it seems a more straightforward way to learn from nature. For example, the animal and plant materials have unique hierarchical structures, and take as a template, the manufacture for engineering piezoresistive architecture will be simplified and can offer tunable elastic modulus, excellent flexibility, and adequate robustness to congruently fit the requirements of e-skin<sup>97</sup>. Inspired by the hierarchical surface of lotus leaf, a multiscale design of piezoresistive sensor based on PDMS obtained a high and stable sensitivity ( $1.2 \text{ kPa}^{-1}$ ) with a wide range of linearity (0–25 kPa) (Fig. 4(b))<sup>98</sup>. In another study, a piezoresistive sensor that replicated the micropapillary of rose petals was to mimic the structures on the human epidermis and dermis and showed an ultra-low detection limit (<2 Pa) to detect multiple life activities (Fig. 4(c))<sup>99</sup>. Based on carbon nanotubes and graphene, Jian et

al.<sup>100</sup> developed a high-performance sensor with a unique piezoresistive design, by a combination between natural leaf structure and aligned artificial geometry. Similarly, Jang et al.<sup>101</sup> proposed a new piezoresistive design for pulse detection, of which the active portion was an irregular micropatterned PDMS negatively replicated from shark skin and sealed with PEDOT:PSS films (Fig. 4(c)). This design resulted in a significant improvement in the sensor's sensitivity over regular artificial patterns. Future efforts on bioinspiration maybe toward the overall enhancement of sensor performances, including manufacture, mechanical property, and sensing function for e-skin application.

### Crack structures

By inspiration from the slit organ in a spider, it is proposed that crack-like structures for the design of piezoresistive sensors, can have unique mechanical compliance due to the effective deformation upon receiving even a small variation in mechanical loading, thereby giving ultrasensitive detection performance. With the absence of applied force, the presence of cracks could reduce the initial current significantly by destruction of conductive paths, and upon loading the cracks tended to coalesce for an enhanced sensing capability<sup>103</sup>. Kang et al.<sup>16</sup> were the pioneers who firstly mimicked a spider's slit organ and fabricated nano-crack junctions for designing piezoresistive sensors. Their findings highlighted the effectiveness of cracks toward an ultrahigh sensitivity ( $\sim 2000 \text{ GF}$  at 2% strain) of the piezoresistive sensor, and opened a window for more investigations on piezoresistive cracks from nano to micro scales. Chen et al.<sup>102</sup> reported a piezoresistive sensor with artificial cracks and suggested a principle for the sensor's high sensitivity due to the cyclic disconnection-reconnection of crack junctions under external strain (Fig. 4(d)). Meanwhile, in order to

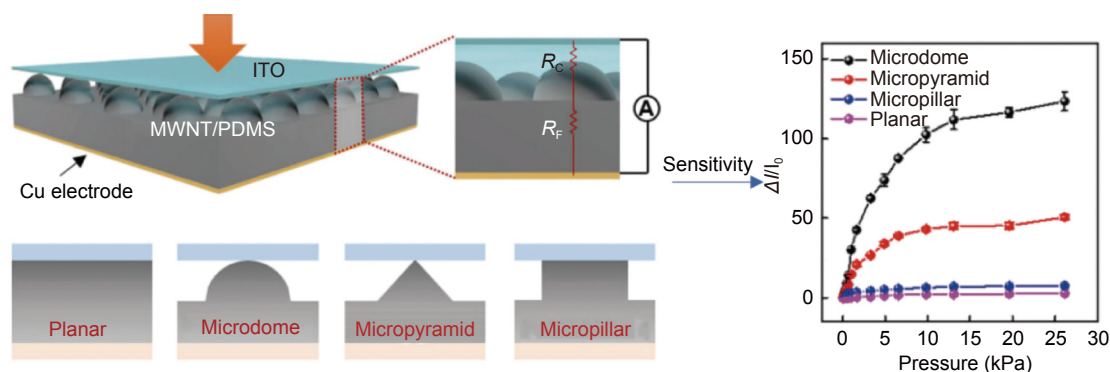


**Fig. 5 | Sensitivities of different microstructure sensors.** ITO, indium tin oxide; MWNT, multiwalled carbon nanotubes; and PDMS, polydimethylsiloxane. Figure reproduced with permission from ref.<sup>94</sup>, under a Creative Commons Attribution 4.0 International License.

facilitate crack fabrication, Yang et al.<sup>104</sup> developed a controlled method for the flexible piezoresistive sensor, by which a pre-stretch of 5% strain on Au coated PDMS resulted in cracks in the conductive coating due to its rigid nature and weak interaction at the interface between metal and polymer. Owing to the cut-through channel cracks, the as-fabricated sensor showed superior GFs at different external strains, e.g.  $GF=200$  for  $\varepsilon<0.5\%$ ;  $GF=1000$  for  $0.5\%<\varepsilon<0.7\%$ ; and  $GF>5000$  for  $0.7\%<\varepsilon<1\%$ . However, applying a large strain to the sensor was found to cause rapid crack propagation and catastrophic coating fracture, which might limit a piezoresistive sensor based on the crack structure for sensing a large-range strain. In order to overcome these problems, Shi et al.<sup>105</sup> developed a simple and scalable bio-templating method, to introduce microcavities in an Au thin film. This method had an effective control on crack patterns, and enhanced the interfacial adhesion between metal and elastomer, thereby offering a high sensing range up to a tensile strain of  $\sim 90\%$  by avoiding crack propagation successfully.

### Combined structures

Nowadays, increasing evidence demonstrates that a combination of different structures can endow a piezoresist-

ive sensor with better performances than the single microstructure alone. The combination gives not only the sensor multi-sensing functionality, e.g. strain and pressure, but also improvements on the overall sensing performances including sensitivity, linearity, detection range, and response time. For example, Ji et al.<sup>86</sup> developed a piezoresistive sensor based on the hierarchical architecture comprising of mesoscale domes and microscale pillar arrays and showed an improved sensitivity of pressure greatly (Fig. 6(a)). Learning from the leaves of *Epipremnum aureum*, Zhao et al.<sup>106</sup> developed a hierarchical architecture that combined macroscale veins and plenty of microscale surface pores (Fig. 6(b)). Compared to the single-structured piezoresistance, this architecture could enable a higher sensitivity for the piezoresistive sensor, due to resistance change from the addition of pores that upon external loading introduced variations in the contact area and conductive path. Another work that replicated banana leaves explored a different hierarchical architecture, comprising of microaligned mountains with secondary and tertiary ridges, and under pressure could obtain additional microcracks to further improve the sensitivity of the piezoresistive sensor<sup>103</sup>. However, replication from the natural

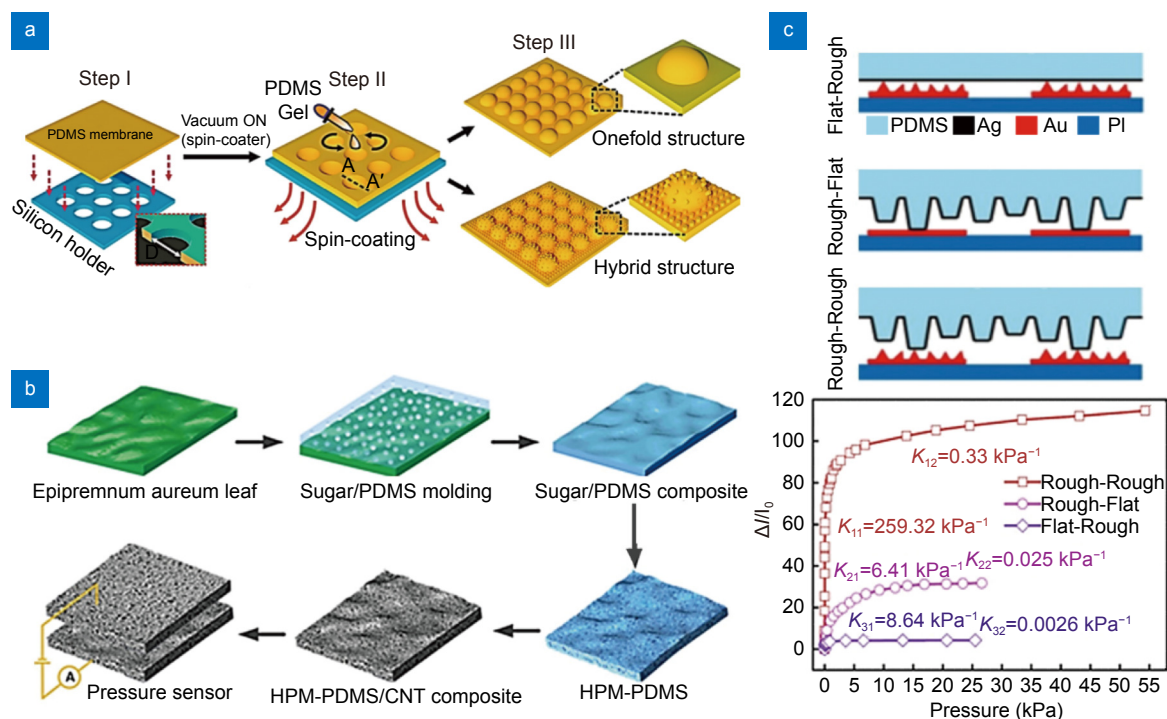


**Fig. 6 | Piezoresistive design and manufacture with hierarchical structure.** (a) Multiple dome structures as piezoresistance sensing layer<sup>86</sup>. (b) Multiple structure comprising of dense protuberances and porous structure as piezoresistance sensing layer<sup>106</sup>. HPM, hybrid porous microstructure; and CNT, carbon nanotubes. (c) Piezoresistive sensitivities based on the sensing layers comprising of rough-to-rough, rough-to-flat and flat-to-rough surfaces<sup>107</sup>. Figure reproduced with permission from: (a) ref.<sup>86</sup>, (b) ref.<sup>106</sup>, (c) ref.<sup>107</sup>, American Chemical Society.

structure is inconsistent and uncontrollable. Chen et al.<sup>107</sup> reported a hierarchical sensor based on the combination of artificially designed PDMS/Ag microstructures (As sensing layer) and polyimide/Au (PI/Au) rough topography (As interdigital electrode; Fig. 6(c)). Due to more contact touchpoints and significantly declined resistance upon loading, the sensor achieved a higher piezoresistive sensitivity than the devices with either a flat sensing layer or smooth electrode, and thus. Similarly, Sun et al.<sup>108</sup> developed a simple and low-cost method for engineering sensitively flexible piezoresistive sensors, by the employment of a pyramid structure and a double-sided rough structure. Because of limitation in the continuous deformation under a high loading pressure, the piezoresistive sensitivity of a hierarchical sensor was usually lower than the single-structured sensor. However, at small pressures, it was found that a hierarchical architecture as the sensing portion could give very high sensitivity, and its detecting range at the high sensitivity was much larger than that of the single-structured sensor.

### Fibrous architecture

Fibre may be an ideal type of piezoresistive structure due to its unique elasticity for e-skin, with the ultra-low light-weight and high length-to-diameter ratio. The piezoresistive fibre can also conform to the geometric variety of different body parts, e.g. wrist and finger<sup>109</sup>. In the fibre form, a piezoresistive sensor can be easily designed from conductive materials, e.g. polymer, carbon, and carbonaceous composite<sup>110,111</sup>. Different from the rigidity of bulk material, fibrous architecture offers the piezoresistive structure that has not only 3D compliant flexibility and stretchability but also a more compressible deformation than 2D materials along the thickness. A fibrous sensor can have longer durability and higher sensitivity, which is probably attributed to an additional piezoresistivity and the more conductive paths upon receiving stretchable/compressive deformation. As such, it is expected to overcome shortcomings related to current e-skin, such as inadequate sensitivity, limited detection stability, less scalability, low mechanical stretchability, poor reproducibility, and wash instability.

### Natural origin of fibres

It is easy to fabricate piezoresistive fibres through integration of fibrous insulator with conductive material by immersion<sup>112</sup>, coating<sup>6</sup>, and *in-situ* growing<sup>113</sup>, where the

fibres could be natural and engineering origination. For example, Zhang et al.<sup>114</sup> reported a piezoresistive pressure sensor, through the layer-by-layer stacking of PDMS and anchored cotton fabric. A treatment of carbonisation was used to endow the cotton fabric a high conductivity, whilst maintaining well the fibrous integrity and flexibility. Cao et al.<sup>112</sup> obtained natural fibres by cutting the cotton clothes directly and soaked them in a solution containing rGO and Ag nanowires to obtain conductivity (Fig. 7(a)). Based on cotton fibres, the piezoresistive sensor upon applying loading stress could have physical contacts between the device upper and lower layers, among which the Ag nanowires as a more efficient and rapid charge channel provided a significant resistance change and high sensitivity for the e-skin. However, from the perspective of long-term use, conductive material falling off from fibres should be preferentially avoided, and the advances in dipping technology would promote low-cost piezoresistive sensors engineering simply and quickly.

### Electrospun fibres

Electrospinning is a typical process for fibre manufacturing, during which polymer solution or melt is jet spun under a strong electric field, and can be stretched into different diameters away from the nozzle tip. It can generate desirable fibres for piezoresistive sensors, with advantages of low cost, simple procedures, and large-area fabrication. Bi et al.<sup>66</sup> reported a fibrous piezoresistive sensor from polyimide (PI) fibres that supported the *in-situ* growth of Ag particles post electrospinning. It responded to external pressures by changing physical contacts among the Ag-modified PI fibres, and this formed the sensor's piezoresistive foundation. Furthermore, the piezoresistive sensor was able to sense temperature change based on an effect known as electron scattering. By integration with a planar PDMS film, Wang et al.<sup>115</sup> electrospun carbonised silk nanofibres to serve as a sensing portion, and thus avoided the complicated procedures required for common surface micropatterning. By this method, the fibre piezoresistive sensor showed good transparency and promising application for future invisible wearables. Using electrospun fibre as supporting, sensing and packaging layers, Zhao et al.<sup>116</sup> obtained a sandwich-structured piezoresistive sensor, to sensitively detect pressure for human motion and vital sign monitoring. The change in fibrous contact points was proposed as the piezoresistive mechanism for sensing

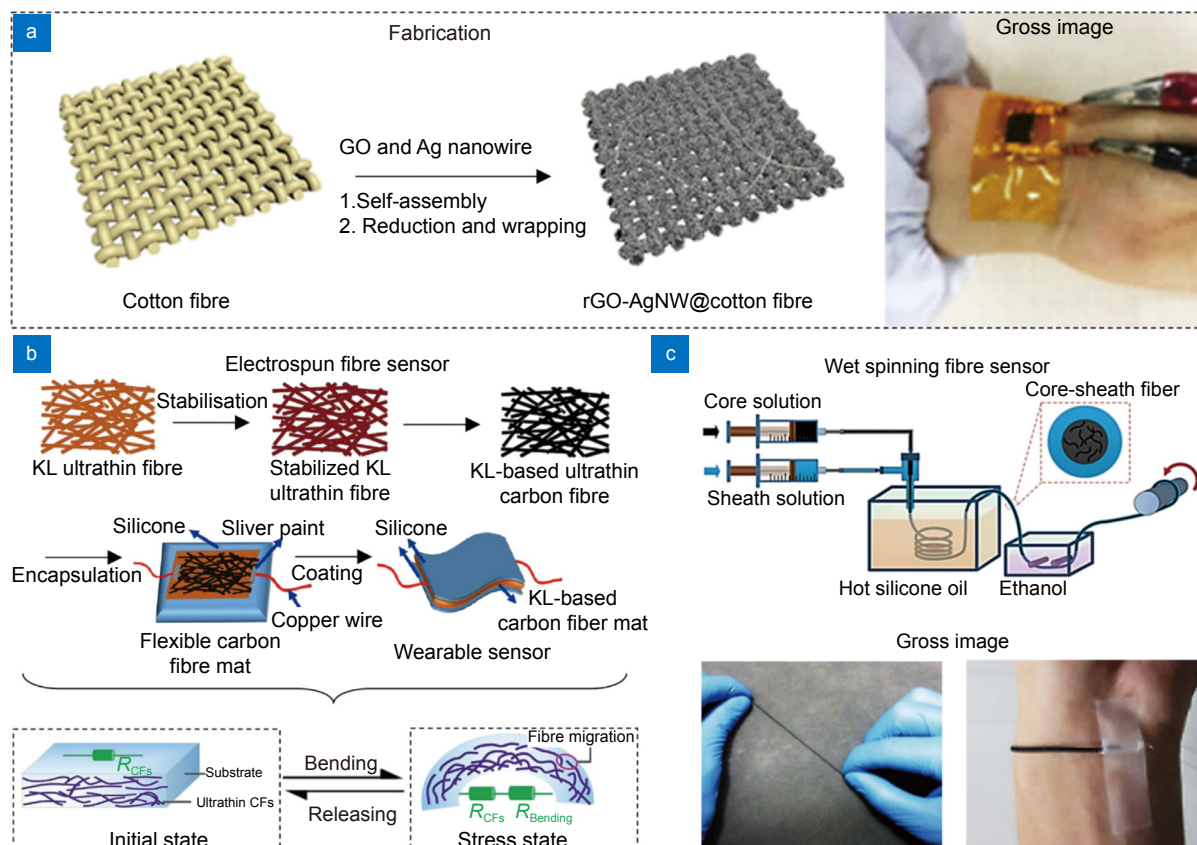


**Fig. 7 | Design and manufacture of fibre piezoresistive sensor.** (a) Schematic of a rGO-Ag NW@cotton fibre, through immersion of cotton fibres in a reductive solution containing GO and AgNW<sup>112</sup>. GO, graphene oxide; rGO, reduced GO; and AgNW, Ag nanowires. (b) Scheme of an electrospun fibre piezoresistive sensor and its sensing mechanisms during pressure and bending<sup>110</sup>. KL, kraft lignin. (c) Scheme of a wet-spinning single-fibre piezoresistive sensor<sup>122</sup>. Figure reproduced with permission from: (a) ref.<sup>110</sup>, (b) ref.<sup>112</sup>, Elsevier; (c) ref.<sup>122</sup>, American Chemical Society.

loading and unloading processes. In line with this, fibre separation would give resistance increase; and based on the principle, Wang et al.<sup>110</sup> developed a piezoresistive sensor using carbon fibre mats to monitor body bending actions (Fig. 7(b)). Future research on electrospun fibres as a conductive portion to offer piezoresistance may have breakthroughs in sensing performance if the limitation in fibre-mat thickness by electrospinning could be overcome.

Electrospun fibre can also serve as a sensor dielectric portion and forms piezoresistance by tailoring the electronic resistance from point-to-point, point-to-face and face-to-face contacting changes. Liu et al.<sup>117</sup> fabricated a piezoresistive sensor that was composed of a dielectronic layer (Electronic polyvinyl alcohol (PVA) nanowires) sandwiched between ultrathin wrinkled graphene films, obtaining excellent piezoresistive sensitivity. Similarly, using electrospun PVA nanowires as a spacer between wrinkled conductive polypyrrole films, Luo et al.<sup>118</sup> assembled a piezoresistive sensor with subtly controlled

conductive paths. Beyond a simple sensing mechanism of conductive path change, the electrospun nanofibers as a spacer enabled the multiple changes of effective contact, leading to higher sensitivity and wider response range. Alternatively, electrospun fibre can be explored to couple piezoresistance with other properties, e.g. piezoelectric, triboelectric and thermoresistive effects<sup>119,120</sup>, for integrated multi-functional sensors.

### Wet spinning fibres

Wet spinning has advantages of facile, fast, low-cost and upscalable fabrication, and is another method of fibrogenesis that finds wide applications in different piezoresistive sensors. Using multi-walled carbon nanotube as conductive fillers and poly(styrene-butadiene-styrene) as a flexible matrix, Yu et al.<sup>121</sup> fabricated a stretchable sensor by wet spinning and obtained a highly stable and sensitive piezoresistance to the applied strain. In a different design, Tang et al.<sup>122</sup> applied wet spinning to generate core-sheath structured fibres (A polymer elastomer

wrapped carbon nanocomposite), which could be used directly as a piezoresistive strain sensor (Fig. 7(c)). Furthermore, Tang et al.<sup>123</sup> realised non-monotonic responsibility for integrated strain and pressure sensing, by a coaxial composite fibre from wet spinning. This piezoresistive sensor overcame the shortcoming of typical fibre sensors that sensed only a single force and could be used to detect blending strain when placed on joint position and external pressure when placed on inactive positions. However, it still requires more efforts for wet spinning to advance the piezoresistive manufacture and extended applications for e-skin.

### Spongy architecture

The 3D architecture from spongy can be designed for piezoresistive sensors, and compared to solid structures it has been reported with improved flexibility for a large-scale sensing application<sup>124</sup>. In principle, the more conductive paths will be formed by the more contact points and areas building temporarily upon the spongy receiving compression; and this leads to material's resistance change and piezoresistance for the detection of transient and static deformations. Piezoresistive spongy sensors can be obtained from conductive materials directly or non-conductive materials in combination with other procedures, e.g. coating, impregnation, blending and carbonisation.

### Direct fabrication of conductive sponges

Different materials have been explored for the conductive sponge fabrication, including carbon materials (carbon nanofiber, carbon nanotube, and graphene), conducting polymers, and even metals<sup>52</sup>. For example, Zhong et al.<sup>125</sup> prepared a wrinkled graphene foam by freeze-drying with the zinc-chloride template and assembled a piezoresistive pressure sensor that had effective interfacial contacts for long-cycle stability and outstanding mechanical resilience. By an ice-template freezing method, a different sensor based on hybrid rGO/MXenes aerogels was developed, with a high piezoresistive sensitivity obtained from the synergistic effect between rGO (Large surface) and MXenes (Conductivity; Fig. 8(a))<sup>68</sup>. However, the low mechanical durability of the sponge might hinder its flexible application in piezoresistive e-skin. To address this problem, Zhai et al.<sup>126</sup> combined unidirectional freeze-drying and ultrasonic dispersion to form aligned pores from elastic materials and achieved excellent recoverability and wonderful

compressibility for piezoresistive application. Using the directional freeze-drying followed by annealing, Zhuo et al.<sup>127</sup> developed a facile fabrication of lamellar aerogel (MXene and cellulose nanocrystals; Fig. 8(b)) that showed extraordinary mechanical performances and ultrahigh linear sensitivity in a broad pressure/strain range. Based on an aerogel comprising carbon nanotubes and cellulose nanofiber layers (Modified with wave-shaped rGO), Peng et al.<sup>128</sup> similarly obtained an ultralight and highly sensitive piezoresistive sensor.

### Indirect fabrication of conductive sponges

Generally, a highly conductive material makes sponges have small resistance change and a limited sensitivity, to sense low-magnitude loadings<sup>129</sup>. In order to serve this problem, different post-procedure, e.g. dip coating and sputtering, to a sponge from non-conductive materials, can be a simple, efficient and straightforward solution that receives extensively investigations in recent years, whilst insulated sponges can have commercialised availability and/or be fabricated efficiently by combining a segregated structure and sacrificial method. For example, Ma et al.<sup>130</sup> reported a piezoresistive sensor by dip-coating the commercialised sponge with graphene and carbon nanotubes, where conductive networks were effectively built on the sponge's skeletons (Fig. 8(c)). Alternatively, Pang et al.<sup>131</sup> coated multilayer graphene on Ni foam and after chemical etching of the metallic template, obtained intact graphene porous networks in PDMS substrate that were capable of detecting piezoresistive changes to pressure and strain (Fig. 8(d)). Using the Ni-based sacrificial template followed with mechanical fracture, Zheng et al.<sup>132</sup> developed a more stretchable and flexible piezoresistive sensor by electropolymerization, and successfully introduced micro-cracks in the foam skeleton for multifunctional detections, e.g. pressure and strain. The Ni-based scarification method was developed further by Luo et al.<sup>82</sup>, where graphene grew on PDMS before Ni etching away. Through this development, the foam conductivity and mechanical properties could be regulated by the number of graphene layers and the composition's ratio, respectively. These accounted for improved sensitivity and a linearly sensing region of the piezoresistive sensor. Different from the metal templates, Sengupta et al.<sup>32</sup> replicated an ultralight-weight and highly squeezable foam from sugar cubes and obtained the piezoresistance by infiltrating the foam with conductive multilayered graphene. Similarly, Zhai et al.<sup>133</sup>

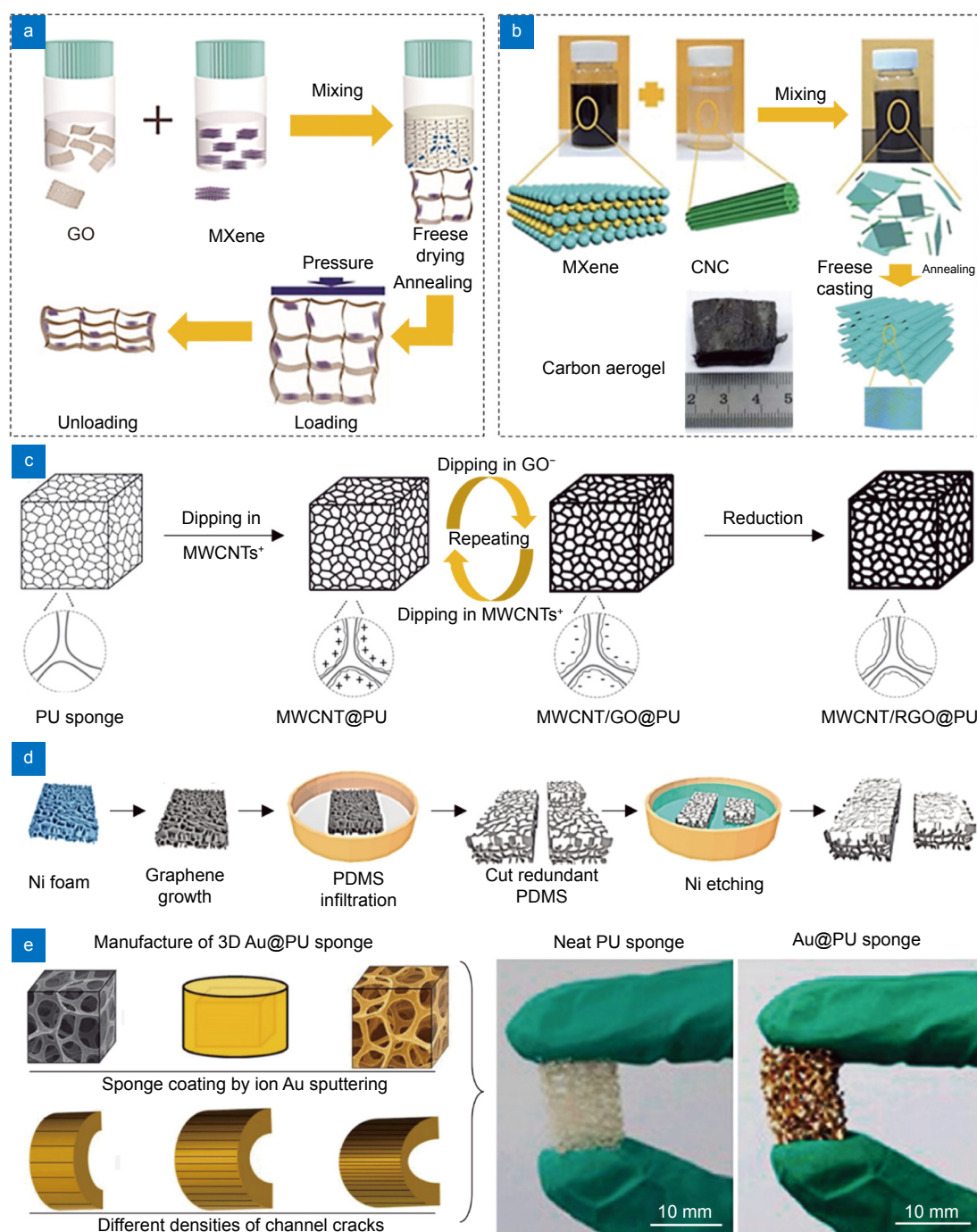


**Fig. 8 | Piezoresistive design and manufacture with spongy structure.** (a) Freeze drying for the fabrication of piezoresistive sponge<sup>68</sup>. (b) Directional freeze drying of the fabrication of piezoresistive wave-shaped sensing layers<sup>127</sup>. CNC, cellulose nanocrystals. (c) Dip coating of as-fabricated sponge with conducting materials<sup>130</sup>. PU, polyurethane; and MWCNT, multiwalled carbon nanotubes. (d) Sacrificial template for the fabrication of piezoresistive sponge<sup>131</sup>. (e) Sponge-based hierarchical structure (e.g. cracks) for piezoresistive sensor<sup>134</sup>. Figure reproduced with permission from: (a) ref.<sup>68</sup>, (d) ref.<sup>131</sup>, (e) ref.<sup>134</sup>, American Chemical Society; (b) ref.<sup>127</sup>, (c) ref.<sup>130</sup>, Royal Society of Chemistry.

used sugar as the sacrificial template of piezoresistive sensing portion, and enhanced the sensor's detection range by building 3D conductive networks from carbon-black-decorated foam.

Translation of piezoresistive sponge sensors, however, is still limited in e-skin, due to the brittle nature of con-

ductive materials and a weak adhesion (Easily peeling off) on sponge insulate skeletons<sup>52</sup>. In order to solve this problem, a new dip-coating approach was developed by the alternate deposition of positively charged chitosan and negatively charged MXene on the surface of existing spongy skeletons, where chitosan served as a “binder” to

enhance the interfacial interaction between MXene sheets and spongy skeletons<sup>33</sup>. Another problem that hinders the sponge's translational application, is its inability to sense small mechanical stimuli and thus generate detectable deformation and conductive path change. The introduction of cracks into the sponge skeleton can be a solution, with the possibility of transforming tiny stimuli into electrical signals. For instance, by the generation of pre-external compression cracks, an Ag/cellulose coated sponge could have the capability for simultaneously detecting both large and small strains<sup>76</sup>. Using ion-sputtering Au decoration, Wu et al.<sup>134</sup> demonstrated a channel crack-based gold@polyurethane sponge, which achieved similar detectability to both tiny mechanical variation and large motion (Fig. 8(e)). In another study, using supercritical CO<sub>2</sub> foaming followed by hydrogen bond assembly, plenty of microcracks were prepared on 3D interconnected conductive channels<sup>67</sup>. The as-fabricated piezoresistive sensor showed high GFs (up to 13.27) when less than 5% compression strain was applied, and in the response, the microcracks contributed to the synergistic effect between disconnect-connect transition. In addition to the conductivity issues, sponges from sacrificial templates were also reported with restricted porosity previously, and in order to solve this problem, researchers developed an emulsion method that could generate highly ordered and tunable pores. For example, in a graphene sponge, the porous structure accounted for excellent elasticity and piezoresistive effects (GF: 0.79–1.46) for potential e-skin application<sup>135</sup>. Furthermore, the poor mechanical durability of insulating sponges might also hinder their real application; and similar to the sponges from conductive materials, this can be solved by directional-freezing to form aligned porous architecture<sup>136</sup>.

### AM-assisted piezoresistive architecture

AM-assisted design and fabrication can advance the development of piezoresistive sensors, by the rapid prototyping of different material architectures as discussed above, e.g. fibre, protrusion, and porous structure<sup>137</sup>. This method allows for a free and customised design of the piezoresistive architecture and sensor shape for specific e-skin application, even with the 3D geometry required a complex and highly precise fabrication<sup>138</sup>. Presently, AM builds a 3D digital model from scanners or computer-aided design software and decomposes the model into a series of Z-direction discrete layers for lay-

er-by-layer printing and 3D construct deposition<sup>139–141</sup>. AM has been used to print piezoresistive sensors with re-determined mechanical performances and functionality, including the structured mold, substrate and sensor body, sensing elements, electrodes and the full sensor.

In principle, AM printing of piezoresistive architecture relies on certain inks, e.g. a blending of rigid conductive materials into flexible polymer matrixes<sup>142</sup>. Furthermore, the high viscosity of inks, e.g. milled carbon fiber/silicone rubber ink, might require a system capable of depositing the ink at high pressure and a high speed, e.g. drop-on-demand AM printing (Fig. 9(a))<sup>143</sup>. Using a nanocomposite liquid suspension, Kwon et al.<sup>31</sup> AM-printed a multi-axial fibre sensor that showed a directly piezoresistive response to the external compression and tensile forces. In another work, Wang et al.<sup>144</sup> developed a printable ink comprising carbon nanotubes and a polymer matrix, of which the carbon nanotube formed an interconnected conductive network for piezoresistive e-skin sensing (Fig. 9(b)). By a printable ink from the carbon nanotube, Si nanoparticle, and silicone elastomer, Tang et al.<sup>145</sup> reported a piezoresistive AM-printing that could have tunability of micropore and conductive network (Fig. 9(c)). Assembling the AM-printed sensor on the fingertips of an ultrathin rubber glove, it realised real-time detection of the grabbing force and different objects, to show a high potential capacity of monitoring and feedback control in future robotics. In contrast, other studies chose the more cost-effective carbon black as conductive materials, in order to have potential industrialisation. For example, Wei et al.<sup>146</sup> reported a homogeneous ink comprising carbon black nanoparticles mixed with Ecoflex0030 at certain ratios for AM printing. Similarly, Wang et al.<sup>147</sup> obtained another ink from carbon black nanoparticles, NaCl (As sacrificial template) and thermoplastic urethane elastomer, for the fabrication of a fully AM-printed piezoresistive sensor. Kim et al.<sup>148</sup> assembled carbon composite and a thermoplastic triblock-copolymer elastomer electrostatically and obtained a low-cost composite dough to enable AM-printing of the piezoresistive sensor with excellent structural control, stretchability, and high sensitivity (GF: 72) and linearity (0.94) (Fig. 9(d)).

It is becoming clearer that AM can enable the tunable fabrication of piezoresistive architecture to meet different design requirements, e.g. size, shape, and geometry. Based on a cubic-structured design, Huang et al.<sup>149</sup> AM-printed a piezoresistive fibre sensor by layer stacking

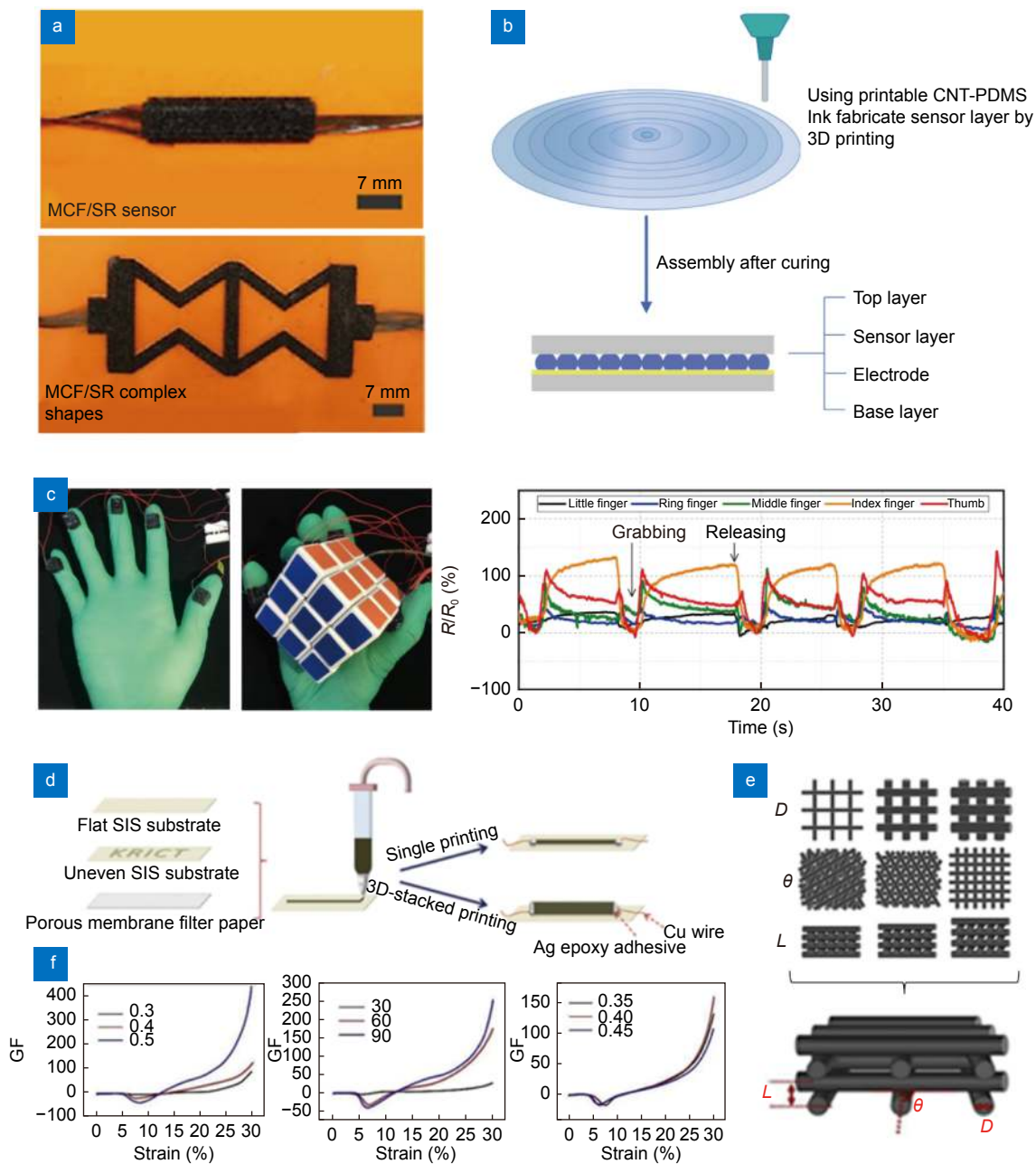


**Fig. 9 | Additive manufacturing for piezoresistive sensor.** (a) Drop-on-demand material jetting for the facial fabrication of piezoresistive structures<sup>143</sup>. MCF, milled carbon fibers; and SR, silicone rubber. (b) 3D printing of human-skin-inspired texture as piezoresistive sensing layers<sup>144</sup>. CNT, carbon nanotube. (c) Application of a 3D printed piezoresistive sensor for robotic fingertips to sense force<sup>145</sup>. (d) 3D printing of conducting composite for piezoresistive sensor<sup>148</sup>. SIS, polystyrene–polyisoprene–polystyrene. (e, f) 3D printing of different structure parameters (e.g. diameter, interaxial angle, and interlayer space) for piezoresistive sensor<sup>149</sup>. GF, gauge factor. Figure reproduced with permission from: (a) ref.<sup>143</sup>, (e, f) ref.<sup>149</sup>, Elsevier; (c) ref.<sup>145</sup>, American Chemical Society; (d) ref.<sup>148</sup>, Royal Society of Chemistry.

(Fig. 9(e) and 9(f)). The parameters of fibre diameter, interfibre angle, and layer height impacted the sensor's GF significantly, and even after experiencing 50% of compressive strain, the sensor could recover quickly with little deformation. Using AM-assisted fabrication, Zhou et al.<sup>150</sup> developed a highly flexible and resistive piezoresistive strain sensor from the commercial resin and Galin-

stan and obtained an asymmetric sensing structure capable of detecting the angle and direction of blending. Furthermore, the AM-assisted fabrication supports scalable piezoresistive architecture, and thus it avoids the complicated assembling steps by traditional methods. For example, using AM-assisted fabrication Guo et al.<sup>140</sup> realised integration of imaging, printing, and multi-

compositional ink optimisation, for the facial fabrication of a stretchable 3D piezoresistive sensor. The optimisation of ink compositions was done through multiple independent nozzles, at the control of different parameter combinations. Possibly, more in-depth development may need a guiding standard for AM-assisted piezoresistive sensors. For different application purposes, the optimisation of printing materials and fabrication procedures is necessary. The manufacturing processes of AM-assisted architecture remain unacceptable for the mass production of piezoresistive sensors<sup>151</sup>.

## Healthcare applications

A clearer picture is emerging that beyond the strain gauge for structural health monitoring and non-destructive testing, the newly development of piezoresistive sensor obtains extensive applications in the e-skin and healthcare field. In this paradigm, the piezoresistive sensor is used for different purposes, such as health monitoring (heartbeat, pulse, and blood pressure), speech recognition, and artificial robots (motion monitoring and control). Such piezoresistive sensors, together with other detections for chemicals and biological signals, can enable multi-functionality towards the early diagnosis of human health and diseases. The following section will focus mainly on the newly emerging applications of piezoresistive e-skin.

### Health monitoring

Signals from respiration, heartbeat, and blood pressure are important physiological indexes of human health. By daily monitoring of the slight variations on these indexes, many diseases can be diagnosed early and treated timely. Meanwhile, macroscopic activities such as daily walking and exercise are also meaningful for healthcare monitoring. For example, gait monitoring in individuals that have sustained pain from Parkinson's disease, stroke, multiple sclerosis, and other neurological conditions, can benefit greatly from daily monitoring on the progression of diseases<sup>32</sup>. Thus, it is becoming accepted that a large detection range of piezoresistive sensors is necessary for e-skin, to monitor physiological indexes in both macroscopic and inferior variations, towards a healthy life, disease prevention, and timely treatment. Additional characteristics that make piezoresistive e-skin able to have information feedback timelier and more overcome the cumbersome defects of existing medical devices, include real-time monitoring, lightweight, easy

to carry, and perfect fitting with human skin.

In order to develop a personally wearable health-monitoring system for the prevention of potential injuries and disease-related disorders, Gong et al.<sup>152</sup> reported a graphene/rGO/polystyrene-based piezoresistive sensor, with adjustable strain range and GF that enabled high sensitivity for the precise detections of the body's posterior cervical pulse and different motion modes (Fig. 10(a)). Guan et al.<sup>153</sup> reported a flexible piezoresistive sensor to detect the physiological signals from the wrist and jugular venous pulse with high sensitivity ( $1.12 \text{ kPa}^{-1}$ ), low detection limit (20 Pa), and ultrawide range (up to 1.2 MPa), which was attributed to a synergistic effect between the nest-like architecture and carbon black percolation network (Fig. 10(b)). Ramírez et al.<sup>154</sup> developed a *de novo* strain sensor using a hybrid architecture from graphene, plasticized PEDOT:PSS, and ultrathin-layered granular palladium, and could detect heartbeat and respiration at the same time, thereby offering the potential to identify a slight difference between the heart rates at breathing and not breathing (Fig. 10(c)). This sensor was for the daily monitoring of obstructive sleep apnea, for the professional medical staff to master the patient's condition and make treatments timely.

Piezoresistive sensors that are designed for the detection of relatively small physiological activities (respiration, heartbeat, and pulse), generally require a very low detection limit and high sensitivity. However, it needs to widen the detection range with proper sensitivity if the sensors aim also to detect large human motions. Tewari et al.<sup>155</sup> developed a MWNT-rGO@PEB piezoresistive strain sensor for the detection of large and small-scale movements of the body. This was achieved by the combination of two different structures, which enabled high sensitivity in a wide detection range and the two linear states at different strain values, e.g. GF 150 for 0–15% strain, and GF 650 for 28–38% strain. Zheng et al.<sup>132</sup> also reported a piezoresistive sensor with excellent performances of high sensitivity and a wide working strain range, for the large-amplitude activity detection including finger bending and wrist movements (Fig. 10(d)). Differently, the performances were achieved based on microcracks on a spongy structure, where the design of cracks was for detecting small-scale activities, e.g. human pulse, and identifying different mechanical stimuli, e.g. pressure force, shear stress, and torsion force.

Further developments show more interest in the

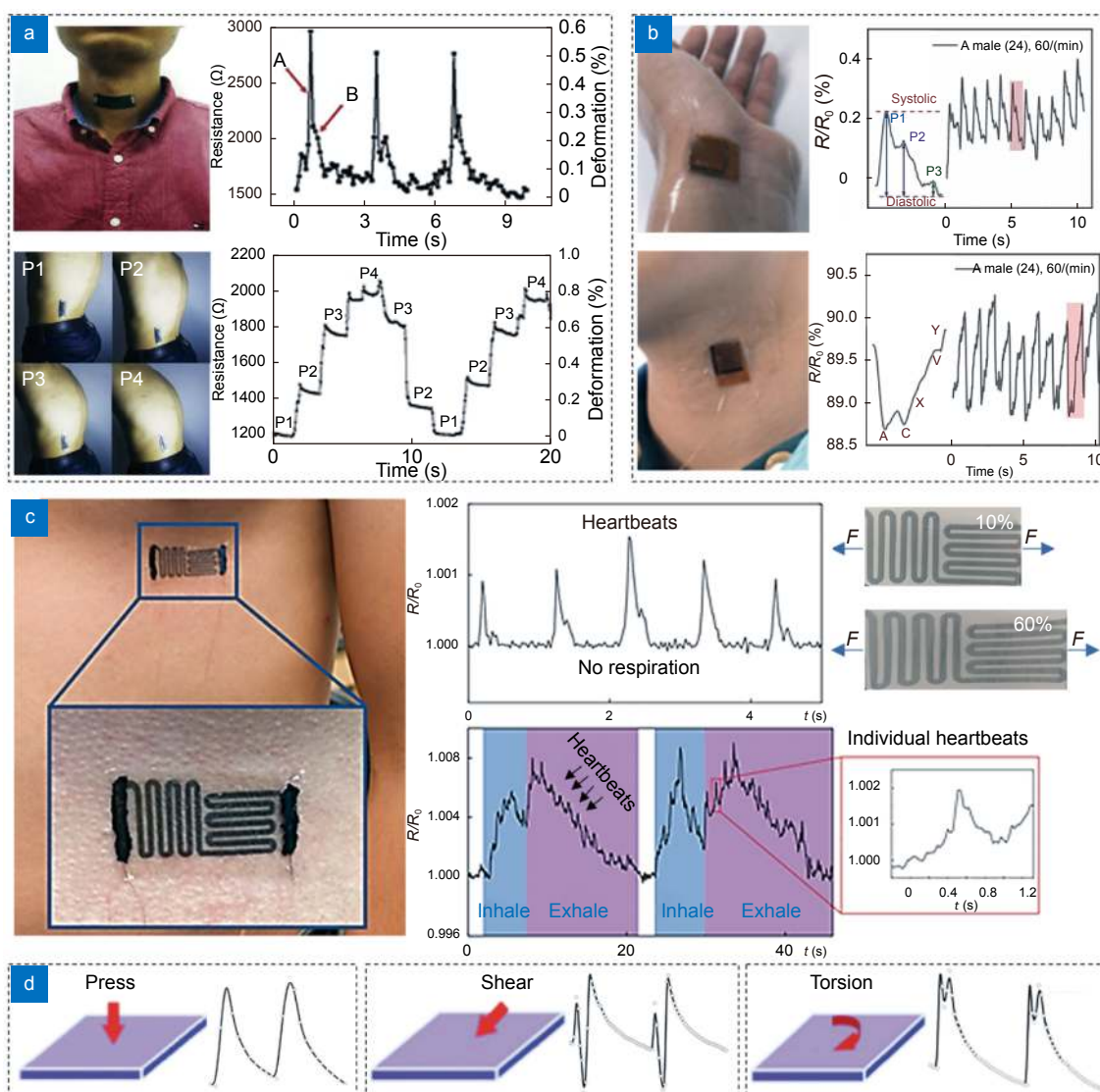


**Fig. 10 | Piezoresistive sensor for health monitoring.** (a) Detection of physical activities by piezoresistive sensor, including the swallowing (A and B: the pharyngeal and esophageal phase, respectively) and the posture of human back<sup>152</sup>. (b) Detection of physiological activities (e.g. wrist and jugular venous pulse) at high sensitivities<sup>153</sup>. (c) Detection of myocardic activities (e.g. heartbeats at breathing and not breathing) by a piezoresistive sensor<sup>154</sup>. (d) Identification of different mechanical stimuli, including pressure, shear and torsion force<sup>132</sup>. Figure reproduced with permission from: (a) ref.<sup>152</sup>, (d) ref.<sup>132</sup>, Elsevier; (b) ref.<sup>153</sup>, (c) ref.<sup>154</sup>, American Chemical Society.

functional integration for health detection, e.g. strain visualisation, alarm and wireless sensing (Fig. 11(a)). For instance, by combining with haptic displays a piezoresistive sensor could be expected to provide the surgeons with haptic pressure feedback and thus, improve the efficacy of minimal access surgery approaches<sup>156</sup>. In another report, Wang et al.<sup>157</sup> developed a piezoresistive sensor that integrated the mechanochromic photon microtubules from interactively full-colour-changeable electronic fibers (Ecoflex/MWCNTs/Ecoflex). As an indicator, the deformation, e.g. strain from 0 to 200% of the fibres could be recorded accurately by the electrical readout. Simultaneously, the photonic crystals generated the

strain feedbacks by instantaneous and reversible colour changes. This integration of multi-functions facilitated a wearable device for real-time monitoring, by digital signals from the resistance and light amplitude changes, as well as colour changes observed intuitively by human eyes.

Piezoresistive sensors have also been investigated for alarm application. Chen et al.<sup>158</sup> developed e-skin from the laser-induced graphene with high sensitivity and integration between detection and alarm function. Design of the piezoresistive effect was for sensing mechanical stimuli, whilst thermoacoustic and excellent acoustic performances were for the detection and alarm function

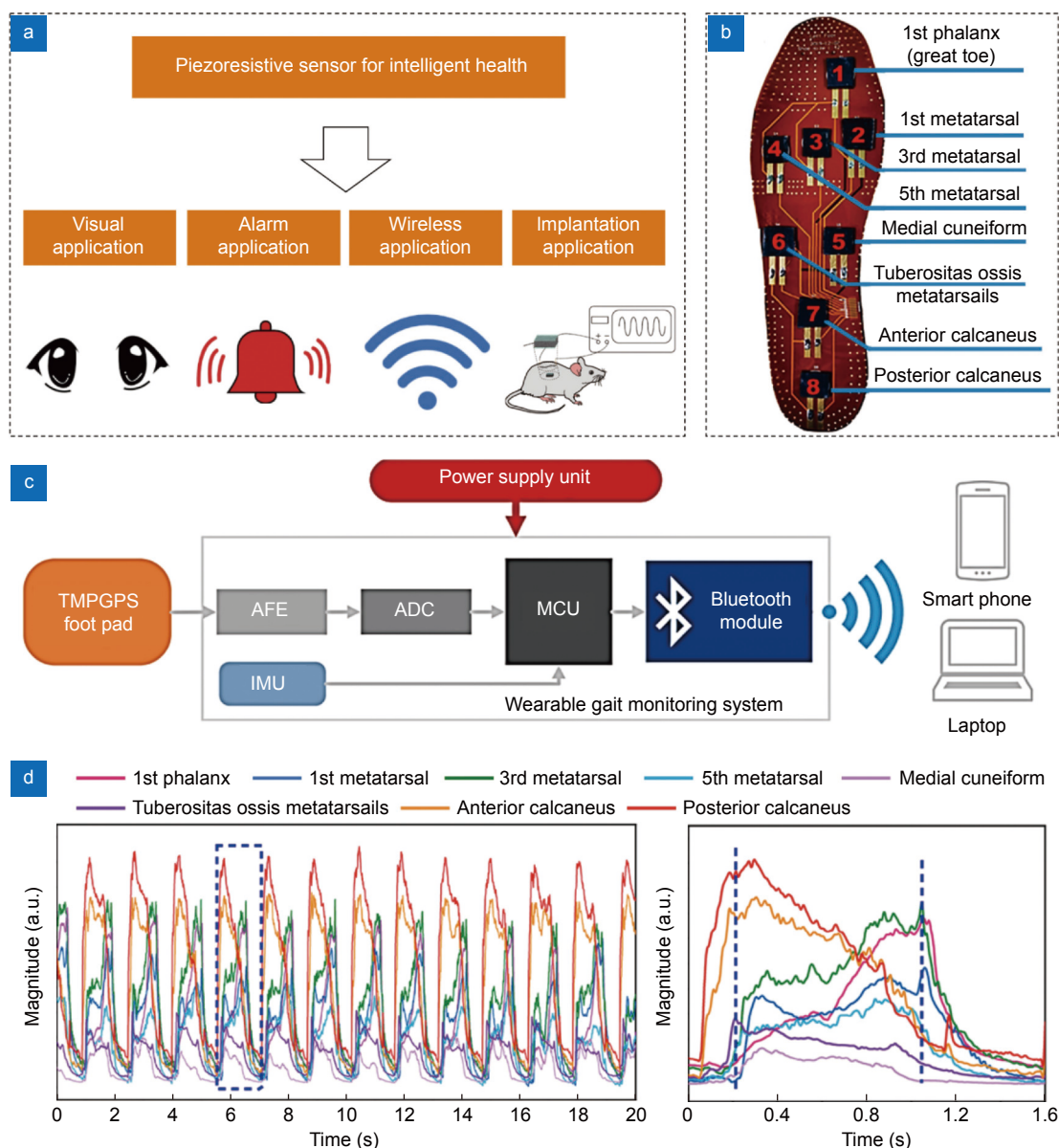


**Fig. 11 | Piezoresistive sensor for intelligent healthcare.** (a) Piezoresistance for visual, alarm, wireless and implanted applications<sup>35</sup>. (b) Triode-mimicking pressure sensor for intelligent shoe pad<sup>159</sup>. (c) Scheme illustrating a monitoring system developed based on the intelligent shoe pad in (b)<sup>159</sup>. (d) Continuous and multiple signals from the integrated gait monitoring system in (c)<sup>159</sup>. Figure reproduced with permission from: (a) ref.<sup>35</sup>; (b–d) ref.<sup>159</sup>, American Chemical Society.

against diseases, such as sleep apnea and cardiovascular diseases. Wu et al.<sup>159</sup> designed a triode-mimicking positive graphene pressure sensor to detect subtle physiological activities and large-scale human activities (Fig. 11(b–d)). Meanwhile, the sensor integrated different functions of signal processing, power management and Bluetooth module. Similarly, Ma et al.<sup>160</sup> fabricated a piezoresistive sensor based on MXene, which accurately recorded blinking and swallowing and sent the signals to a Bluetooth system for portable application. In another work, Wu et al.<sup>35</sup> reported a sponge piezoresistive sensor

for implantation. The sensor exhibited excellent sensing performances for the detection of human activities, e.g. walking motions, and it showed good histocompatibility *in vivo* and a high potential to dynamically monitor nerve repair process without sacrificing animals as required by traditional biomedical evaluations.

### Speech recognition

Presently, speech recognition is used widely in human-computer interaction, such as the voice-controlled electrical operation and the speech-text conversion in

mobile devices (Fig. 12(a)). Instead of sensing the sound waves directly, most sensors detect the movements of the throat by vocal cord vibration and muscle stretching and contraction. This forms the basis of speech recognition by a highly sensitive piezoresistive sensor pasted at the throat<sup>161</sup>. The opposite application of such voice monitoring by piezoresistive sensors made e-skin promising candidates for potential speech recovery via human-machine interaction<sup>103</sup>.

Zhang et al.<sup>162</sup> developed a piezoresistive sensor for voice identification, including different words, vibration, and loudness of the sound (Fig. 12(b)). This was based on the heterogeneously structured MXene for the real-time sensing of low-magnitude vibrations. The force from acoustic vibration was distinct at different volumes,

and based on the piezoresistive effect, it gave electrical signal changes to detect sound loudness. Based on the piezoresistive design, Yu et al.<sup>163</sup> AM-printed a thinner voice device (2 mm in thickness) and attached it to the throat for detecting vocalizations such as tester's speak and cough. The speech induced throat vibration and in turn resistance change in the sensor. At different loudness on intonations or coughs, the same word accordingly gave differences in the peak magnitudes of curves whilst retaining the similar waveforms. This suggested that the waveform could be a recognisable characteristic of a specific word, while the wave details as the recognition of different person's voices, leading to prospects promising for voice recognition in future e-skin.

However, the detection of timbre requires high

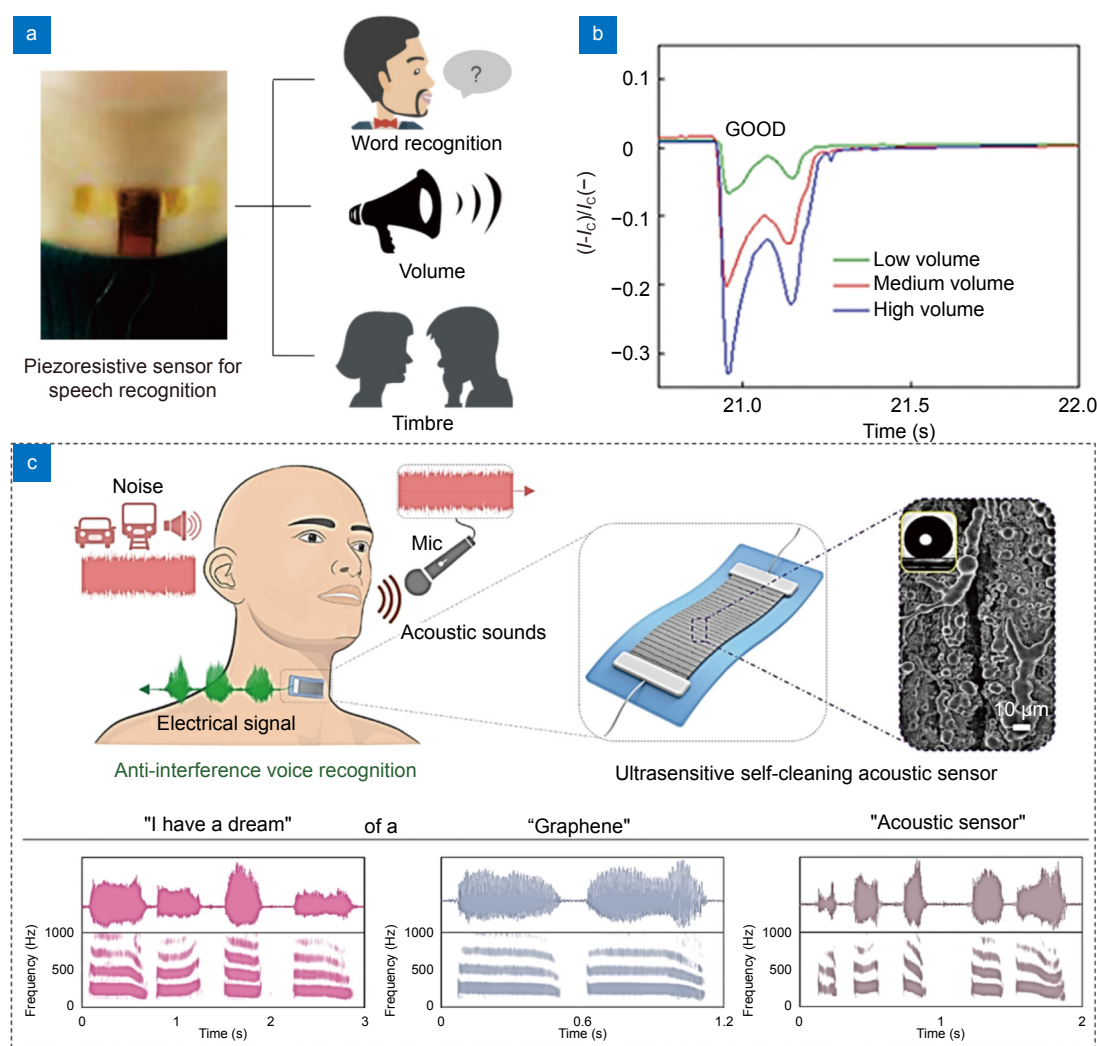


**Fig. 12 | Piezoresistive sensor for intelligent speech recognition.** (a) Piezoresistive detection of sound (e.g. word recognition, volume detection, and voice recognition)<sup>68</sup>. (b) Response of a MXene-based piezoresistive sensor to the audio outputs at different volumes<sup>162</sup>. (c) Anti-interference voice recognition by a skin-attachable piezoresistive sensor<sup>165</sup>. Figure reproduced with permission from: (a) ref.<sup>68</sup>, (b) ref.<sup>162</sup>, (c) ref.<sup>165</sup>, American Chemical Society.

sensitivity and short response time, and the natural frequency of most materials cannot keep up with the vibration of sound waves. Deng et al.<sup>164</sup> achieved timbre recognition by the detection of sound frequency, via an ultra-sensitive piezoresistive sensor comprising of vertical graphene with a high density of cracks at different directions. Furthermore, by the piezoresistive design, Dinh et al.<sup>165</sup> reported a skin-attachable acoustic sensor to avoid background noise interference (Fig. 12(c)). The superior sensitivity ( $GF=8699$ ) of the sensor allowed for the direct capture of small acoustic vibrations, leading to the elimination of background noises.

In fact, the piezoresistive sensor to directly feel sound waves requires even high sensitivity and a very low detection limit. Based on the combination of microscale patterns and cracks, Nie et al.<sup>103</sup> reported a piezoresistive sensor with high sensitivity, which enabled the detection of speech-induced air burst and thus allowed for non-contact speech recognition (e.g. the pronunciation of different single letters). Gao et al.<sup>166</sup> designed the microchannel-confined MXene for engineering a piezoresistive sensor for microforce detection. The sensor to feel sound waves was by the piezoresistive response to pulse forces generated on the sensor's surface, and thus it was able to distinguish different ringing tones at high accuracy in the source waveform outline. Based on MXene@chitosan@polyurethane composition, Li et al.<sup>33</sup> reported a non-contact strain sensor to sense knocking sound quickly (response time: ~19 ms). When a word of 'carbon' was spoken, the sensor was able to identify the two characteristic peaks corresponding to the roots of 'car' and 'bon', respectively. This indicates the potential of the piezoresistive sensor for recognising word pronunciation. However, in the field of speech recognition, there still lacks a standard on piezoresistive design for e-skin. For example, it remains unclear what kinds of signal change corresponding to the specific word. Probably, the human eardrum offers us an opportunity to fully understand how the piezoresistive sensor should be engineered. Future research to convert the signals from key voice characteristics in a standard manner will make piezoresistive e-skin more applicable for speech recognition.

### Prosthetic and artificial robots

Robotic prosthetics and hands require a tactile ability for comfortable and more desirable operations. Under the control of a motion sensor and electrotactile stimulation,

robot hands could be programmed for grasping actions. However, as the substitute of human hands, existing robots were found with issues such as inaccurate capture, the poor control of strength, and a limited diversity of movement<sup>167</sup>. Recently, researchers have developed piezoresistive sensors to help robots obtain capabilities of tactile feeling and static distance detection, to sense different objects, textures, and positions in order to avoid a collision for better safety and compliance. For example, Dong et al.<sup>168</sup> integrated a piezoresistive strain sensor into intelligent gloves and by signal recognition and feedback, realised movement control on a manipulator. In another study, Liu et al.<sup>169</sup> manipulated robot arms playing music by gestures, where successful human-computer interaction was built between the robotic arms and a piezoresistive sensor (Fig. 13(a)). Xu et al.<sup>83</sup> designed a competitive robot that integrated five independent sensors in the rubber gloves for intelligent human-computer interaction, and the piezoresistive sensors made input characters be highly recognisable. With soft porous and elastic piezoresistive sensors, Sencadas et al.<sup>170</sup> developed a gripper to grasp objects with different shapes and textures. The gripper received signal changes when clamping and releasing objects, and matched closely the sensing characteristics of human fingertips based on the compliant contact detection between fingertips and objects.

Large-area detection of pressure and pressure distribution is another very important robotic capability. The strategies that sense surface pressure by the integration of multi-sensor arrays become challenging, due to the difficulties to apply sensor arrays on a large-scale surface, e.g. plenty of sensor units, big-task signal processing, and lots of connecting wires<sup>166</sup>. Fibres fabricated from conductive poly(vinyl alcohol-co-ethylene) were reported with good piezoresistive properties, and a sensor based on the fibrous mats could sense stress change upon irregular touch, map spatial pressure distribution, and display the contacting object shape (Fig. 13(b))<sup>171</sup>. Liang et al.<sup>172</sup> integrated the e-skin with a piezoresistive sensor and time-of-flight sensor for nursing robot application. The piezoresistive sensor could help the robot to exam object weight and adjust the arm to avoid improper posture (incorrect position) or mechanical failure (excessive weight) for possible slipping. In a different manner, a piezoresistive pressure sensor was applied to the surgical robots for ensuring surgical safety (Fig. 13(c))<sup>173</sup>. This sensor made surgeons avoid unnecessary surgical injury

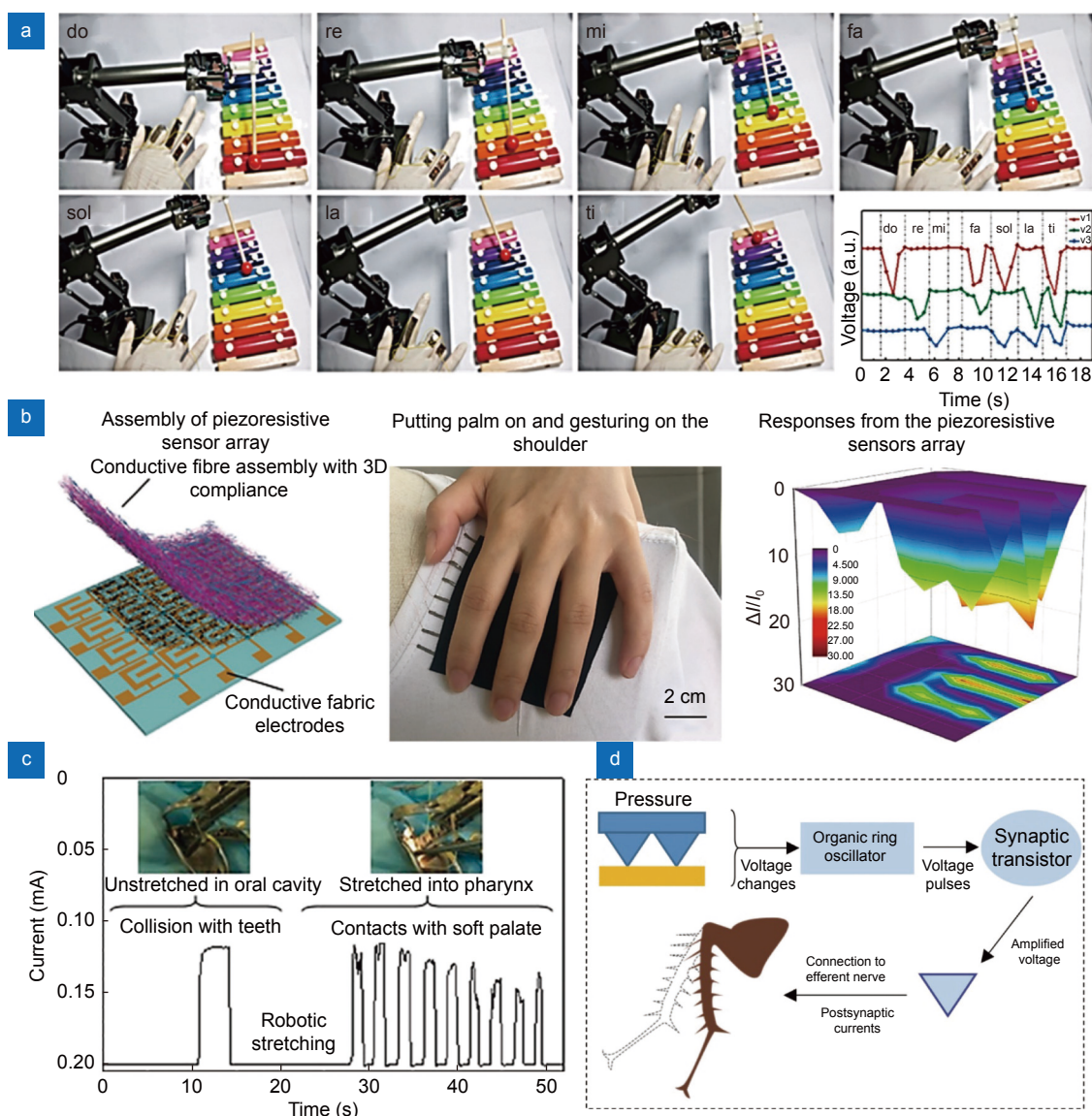


**Fig. 13 | Piezoresistive sensor for prosthetics and robots.** (a) Manipulating the robot arm by a piezoresistive sensor for music playing<sup>169</sup>. (b) Large-area force distribution detected by fibre piezoresistive sensor array<sup>171</sup>. (c) Piezoresistive sensor for the real-time monitoring of robot–tissue collision/interaction in surgical robots<sup>173</sup>. (d) Development of an artificial afferent nerve based on multiple piezoresistive sensors<sup>175</sup>. Figure reproduced with permission from: (a) ref.<sup>169</sup>, (b) ref.<sup>171</sup>, (c) ref.<sup>173</sup>, American Chemical Society.

by improving the awareness of robot-tissue collisions.

Prosthetic limbs are mostly used to recover the self-care abilities of disabled patients; however, their long-term adaptation tends to cause high possibilities of harm to the patients<sup>33</sup>. Piezoresistive tactile sensors that are integrated with the prosthetic limbs can increase the ownership of those patients to feel the external objects and obstacles, increase their natural feeling, and thus adapt better to the existence of prosthetic limbs<sup>23</sup>. Specifically, messages from the sensor stimulate the residual sensory pathways and in turn, alleviates the prevalent phantom limb pain. The piezoresistive feedback from a prosthetic limb not only promotes the patient’s ownership but also

allows for the more natural and facile operation through restoring information about their body position and grip forces. Ferreira et al.<sup>174</sup> fabricated an array of piezoresistive sensor units and connected them to a data acquisition system that had a wireless data transmission capability, to measure the interface pressure and pressure distribution of prosthetic alveolar. With help from the sensors, it became possible to analyse pressure distribution during the socket production process, thereby improving the performances of prosthetic alignment and training with comfort feeling for the patients. Similarly, Kim et al.<sup>175</sup> developed an artificial afferent nerve that integrated with different elements (e.g. the piezoresistive

**Table 1 | Summary on the parameters of current piezoresistive sensors.**

Structure	Materials	Sensor thickness	Performance				Flexible/stretchable	Application/ Force application	Fabrication technique	Ref.
			Sensitivity or GF	Sensing range	Response time	Cyclic test				
Simple "bulk"	CNTs/FKM	100 ~ 300 mm	$1.3 \times 10^5$ ( $\epsilon = 100\%$ )	232% $\epsilon$		500 times Hysteresis (0~150% $\epsilon$ )	Strain/Human motion monitoring and Stretchable LEDs	Internal melt-mixer	ref. <sup>50</sup>	
	SiC/Ecoflex		$2.47 \times 10^5$ ( $\epsilon = 2.5\%$ )	0.05% ~ 5% $\epsilon$		10000 times Consistent (0~4% $\epsilon$ )	Strain and pressure/Health and motion monitoring	Laser direct writing	ref. <sup>65</sup>	
	rGO/PS	~ 60 mm	250 ( $\epsilon = 1.05\%$ )		100 ms	2000 times Consistent (0~0.7% $\epsilon$ )	Pressure/Human movement behaviors	Laser scribe	ref. <sup>52</sup>	
Simple "bulk"	VGr/PDMS		$72(\epsilon = 20\%)$ 22000 ( $\epsilon = 100\%$ )	$\epsilon = 100\%$ (Max)		1000 times Consistent (0~40% $\epsilon$ )	Strain/Human's activities and timbres	Deposition	ref. <sup>64</sup>	
Fibre	rGO-Ag NW@cotton fiber		$4.23 \text{ kPa}^{-1}$ ( $P = 2.0 \text{ kPa}$ )		220 ms		Pressure, bending and twisting/Finger motion and pulse monitoring	Coating	ref. <sup>112</sup>	
Nano fibre	PI@Ag		$1400 \text{ kPa}^{-1}$ (5~100 kPa)	100 Pa ~ 100 kPa	200 ms	1000 times Consistent (5 kPa)	Pressure/Movement of body and temperature	Electrospinning and in situ growth	ref. <sup>66</sup>	
Nano fibre	CSilkNM	$0.63 \pm 0.14 \text{ mm}$	$34.47 \text{ kPa}^{-1}$ (0.8 ~ 400 Pa)	0.8 Pa ~ 5 kPa	16.6 ms	10000 times Consistent (2.5 kPa)	Pressure/Human physiology monitoring and pressure distribution	Electrospinning	ref. <sup>115</sup>	
Fibre	MWCNT/Si/EcoFlex	1.35 mm	1378 ( $\epsilon=330\%$ )	50% ~ 300% $\epsilon$	295ms	10000 times Consistent (0~1000% $\epsilon$ )	Strain, bending and torsion /Human motion detection	Wet spinning	ref. <sup>122</sup>	
Nano fibre	PPy/EVOH/ POE	~ 70 $\mu\text{m}$	$2.83 \text{ kPa}^{-1}$ (0 ~17 kPa)	Upper limit 80 kPa	3 ms	4500 times Consistent (0~10 kPa)	Pressure/Large area pressure sensing	Direct melt extrusion	ref. <sup>171</sup>	
Micro-dome	rGO@NiNWs/EcoFlex		$1302.1 \text{ kPa}^{-1}$ (0 ~ 2.5 kPa)	72 Pa ~ 20 kPa	6 ms	20000 times Consistent	Pressure/Health and motion monitoring	Hot embossing	ref. <sup>80</sup>	
Pyramid	SWCNTs/ PDMS	~ 700 mm	$8655.6 \text{ kPa}^{-1}$ (400 ~ 800 Pa)	Lower limit 7.3 Pa	4 ms	10000 times Consistent	Pressure/Health care	Photolithography	ref. <sup>91</sup>	
Pyramid	PDMS/Carbon	~ 1 mm	$-2.5 \text{ kPa}^{-1}$ (0 ~ 160 Pa)	15 Pa ~ 9 kPa	~20 ms		Pressure/Human movement behaviors	Laser	ref. <sup>7</sup>	
Hierarchical	PDMS/Gr	~ 1 mm	$1.2 \text{ kPa}^{-1}$ (0.2 ~ 25 kPa)	5 Pa ~12 kPa		1000 times Consistent (1.5, and 10 kPa)	Pressure /Human movement behaviors and voice recognition	Soft lithography	ref. <sup>96</sup>	
Micro-papillae	Cu - Ag NWs/ PDMS	~ 1 mm	$1.35 \text{ kPa}^{-1}$ (0 ~ 2.0 kPa)	2 Pa ~ 20 kPa	36 ms	5000 times Consistent (0 ~2 kPa)	Pressure/Human physiology monitoring	Soft lithography	ref. <sup>99</sup>	
Hierarchical	ACNT/Gr/ PDMS	~ 500 mm	$19.8 \text{ kPa}^{-1}$ (0.6 ~ 300 Pa)	0.6 Pa ~ 5.8 kPa	16.7 ms	35000 times Consistent (0~ 150 Pa)	Pressure, bending and torsional/Voice recognition	Soft lithography	ref. <sup>100</sup>	

**Table 1 (Continued)**

Structure	Materials	Sensor thickness	Performance				Flexible/stretchable	Application/ Force application and voice recognition	Fabrication technique	Ref.
			Sensitivity or GF	Sensing range	Response time	Cyclic test				
Surface structure	Crack	~ 10 mm	2, 000 ( $\epsilon = 2\%$ )				Yes/Yes	Depositing/Stretching	ref. <sup>15</sup>	
	Crack	100 $\mu\text{m}$	200 ( $\epsilon < 0.5$ ) 1000 ( $0.5\% < \epsilon < 0.7\%$ ) 5000 ( $0.7\% < \epsilon < 1\%$ )	2% $\epsilon$			Yes/Yes	Depositing/ Stretching	ref. <sup>104</sup>	
	Skin Texture	CNTs/PDMS	2.08 $\text{kPa}^{-1}$ (0.12 $\text{kPa}$ )		50 ms	8000 times Consistent	Yes/Yes	3D-printing	ref. <sup>144</sup>	
	Papillae	SWNT- MXene	11.47 $\text{kPa}^{-1}$ (13 Pa ~ 0.77 $\text{kPa}$ )	(13 Pa ~ 10 $\text{kPa}$ )	20 ms	10000 times Consistent (0~ 1 $\text{kPa}$ )	Yes/No	Etching and exfoliation	ref. <sup>102</sup>	
	Cracks	rGO/PDMS	8699 (0.8 ~ 1.0% $\epsilon$ )	0.000064% (Mim)	107 ms	1000 times Consistent (0~0.35% $\epsilon$ )	Yes/Yes	Femtosecond laser direct writing	ref. <sup>165</sup>	
Porous	Porous	PUI/Liquid metal	>25		202 ms		Yes/Yes	Coating	ref. <sup>46</sup>	
	Porous	Mxenes /rGO	22.56 $\text{kPa}^{-1}$ (1 $\text{kPa}$ ~ 3.5 $\text{kPa}$ )	Lower limit 10 Pa	<200 ms	1000 times Consistent (0~ 0.81 $\text{kPa}$ )	Yes/Yes	Ice - template freezin	ref. <sup>68</sup>	
	Multilayer	Mxenes/CNCs	114.6 $\text{kPa}^{-1}$ (0.05 ~ 10 $\text{kPa}$ )	Lower limit 1.0 Pa	189 ms	2000 times Consistent (0~50% $\epsilon$ )	Yes/Yes	Directional freezing	ref. <sup>127</sup>	
	Porous	Gr/PDMS	0.09 $\text{kPa}^{-1}$ (0 ~ 1000 $\text{kPa}$ )	Upper limit 2000 $\text{kPa}$	100 ms		Yes/Yes	Sacrificial template	ref. <sup>131</sup>	
	Porous	Gr/PDMS	15.9 $\text{kPa}^{-1}$ (0 ~ 60 $\text{kPa}$ )		1.2 ms		Yes/Yes	Sacrificial template	ref. <sup>82</sup>	
	Porous	CNTs/ SiNPs/ Si elastomer polymer	0.096 $\text{kPa}^{-1}$ (0 ~ 175 $\text{kPa}$ )			10000 times Consistent (0- 20 $\text{kPa}$ )	Yes/No	3D - printing	ref. <sup>145</sup>	
	Porous	TPU/CB	5.54 $\text{kPa}^{-1}$ (10 Pa ~ 800 $\text{kPa}$ )	10 Pa ~ 800 $\text{kPa}$	20 ms	10000 times Consistent (40~200 $\text{kPa}$ )	Yes/No	3D - printing	ref. <sup>147</sup>	
	Porous	TPU/CB	1.12 $\text{kPa}^{-1}$ (20 Pa ~ 60 $\text{kPa}$ )	20 Pa ~ 1.2 MPa	15 ms	10000 times Consistent (0- 30 $\text{kPa}$ )	Yes/Yes	Sacrificial template	ref. <sup>153</sup>	

**Table 1 (Continued)**

Structure	Materials	Sensor thickness	Performance				Flexible/stretchable	Application/ Force application	Fabrication technique	Ref.
			Sensitivity or GF	Sensing range	Response time	Cyclic test				
Porous	Multilayer	Gr/Ecoflex	4.68 kPa <sup>-1</sup> (0 ~ 150 kPa) 11.09 kPa <sup>-1</sup> (150 ~ 200 kPa)	Upper limit 200 kPa		1000 times Consistent (0~ 200 kPa)	Yes/Yes	Pressure/Physiological signal detection	Laser scribe	ref. <sup>69</sup>
	Multilayer	Ti <sub>3</sub> C <sub>2</sub> -MXene/PI	180.1 ~ 94.8 (0.19 ~ 0.82% ε)		30 ms	4000 times Consistent (0~ 7.5 kPa)	Yes/Yes	Pressure and strain/Human's activities	Etching	ref. <sup>60</sup>
	Multilayer	GO/Gr	0.032 kPa <sup>-1</sup> (< 1 kPa)			8000 times Consistent	Yes/Yes	Human computer interaction/Pressure	Ultrasonic	ref. <sup>69</sup>
Combined structures	Hybrid	AgNWs/PDMS	128.29 kPa <sup>-1</sup> (0 ~ 200 Pa) 1.28 kPa <sup>-1</sup> (0.2 ~ 10 kPa)	2.5 Pa ~ 8.0 kPa	<100 ms	10000 times Consistent (0~ 10 kPa)	Yes/No	Pressure/Human physiology monitoring and voice recognition	Laser etching	ref. <sup>86</sup>
	Textured@Porous	CNTs/PDMS	83.9 kPa <sup>-1</sup> (<140 Pa)	0.5 Pa ~ 10 kPa	170 ms	29000 times Consistent	Yes/No	Pressure/Human physiology monitoring and voice recognition	Soft lithography/sacrificial template	ref. <sup>106</sup>
	Conical frustum-like structures	Ag/PDMS	259.32 kPa <sup>-1</sup> (0.36 Pa ~ 2.5 kPa)	0.36 Pa - 54 kPa	200 μs	1000 times Consistent (0~ 0.47 kPa)	Yes/No	Pressure/Health monitoring and intelligent robots	Lithography/Deposition	ref. <sup>107</sup>
Others	Crack @Porous	PANI/PDMS	~0.055 kPa <sup>-1</sup> (4 Pa ~ 5 kPa) 10 (ε = 25%)	Lower limit 4 Pa	60 ms	500 times Hysteresis (0~5% ε)	Yes/Yes	Pressure, strain, shear and torsion/Human movement behaviors	Sacrificial template /Stretching	ref. <sup>132</sup>
	Crack @Porous	Gold@PU	59 ~ 122 Pa <sup>-1</sup> (0 ~ 14.2 kPa)	Lower limit 0.568 Pa	9 ms	1000 times Consistent (0~45% ε)	Yes/Yes	Pressure/Voice recognition and vehicle speed calculation	Ion sputtering/Compress	ref. <sup>134</sup>
	Sandwich	PEDOT:PSS/AgNWs/PDMS	8.0 (ε = 40%) 4.52kPa <sup>-1</sup> (0 ~ 3 kPa) 28.34kPa <sup>-1</sup> (3 ~ 10 kPa)	50% ε (Max)		300 times Consistent (0~30% ε)	Yes/Yes	Strain/Finger motions	Transfer - printing technique	ref. <sup>74</sup>
Sandwich	WGF/PVA/PI		2.24 Pa ~ 14 kPa	87 ms	6000 times Consistent	Yes/Yes	Pressure/Human movement behaviors	Electrospinning and ink - jet-print	ref. <sup>117</sup>	

GF: gauge factor (in some case just a single-point value).

CNTs: carbon nanotubes; FKM: fluoroelastomer; SiC: silicon carbide; MWCNTs: multi-walled carbon nanotubes; Si: silicone; CB: carbon black; PDMS: polydimethylsiloxane; rGO: reduced graphene oxide; PS: polystyrene; VGr: vertical graphene; Ag NW: silver nanowire; PI: polyimide; Ag: silver; CSiKMM: carbonized silk nanofiber membranes; PPy: polypyrrole; EVOH: poly(vinyl alcohol-co-ethylene); POE: polyolefin elastomer; NINWs: nickel nanowires; SWCNTs: single walled carbon nanotubes; Gr: graphene; ACNT: aligned carbon nanotub; Pt: platinum; PUA: polyurethane acrylate; PU: polyurethane; CNCs: cellulose nanocrystals; SINPs: silica nanoparticles; TPU: thermoplastic polyurethane; CB: carbon black; PANI: polyaniline; PEDOT:PSS: poly(3,4-ethylenedioxythiophene); poly(styrenesulfonate); WGF: wrinkled graphene film; and PVA: polyvinyl alcohol

pressure sensor, organic ring oscillator, and synaptic transistor; Fig. 13(d)), and realised the connection to biological efferent nerves and showed the information flow to actuate the tibial extensor muscle in the leg.

## Concluding remarks and future prospects

Rapid developments on piezoresistive sensors promote e-skin for prosperous applications, with verified functionality towards high sensitivity, fast response and large detection range. As what we reviewed here, the advances in structural design beyond material composition of a piezoresistive sensor may open a promising window for e-skin, thereby becoming one preferred choice for sensor development. Increasing evidences have suggested that a hierarchical design can give often optimal piezoresistive performance over single structure. However, the fabrication with multiple and complex processes faces obstacles towards a facile integration of piezoresistive structure at different dimensions and materials. Meanwhile, future piezoresistive sensors request flexibly ultrathin and ultralight sensing structure. Luckily, additive manufacturing that gets rapid development in recent years may offer possible solutions for advanced piezoresistive sensors. Next-generation of the piezoresistive sensors should further upgrade without a doubt at the functional performances. Future work along this research direction requires solutions to address inevitable problems including (a) to pursue high sensitivity whilst avoiding interference noise, (b) to pursue long-term performance against any damage and (c) to pursue wireless signal transmission and power supply. Presently, the piezoresistive sensor finds a wide application in various wearable devices. However, its portability is limited greatly due to the leads and external power supply. The recent developments on triboelectric nano generators offer a possible solution<sup>176</sup>, which can allow for a functional integration with the piezoresistive sensor in wearable devices. Meanwhile, the wireless self-power and signal transmission can be another feasible solution<sup>177,178</sup>. This can enable the piezoresistive sensor with portable sensing performance within an available distance.

Another possible research direction for future work is bioadaptability which shall enlarge translational feasibility of a piezoresistive sensor. As reviewed in this work, the metals and semiconductors studied extensively for traditional strain sensors require the additional flexible designs for e-skin application. Fundamentals such as percolation theory and tunneling effect can guide the de-

velopment of different conductive composites at flexibility. The presence of conductive polymer composites represents one of the great breakthroughs in the development of flexible piezoresistive sensors. Unfortunately, increasing reports deliver concerns on the anaerobic infection and inflammation due to a long-term interfacial contact between the polymer and skin. However, challenging issues remain not yet solved completely. In this paradigm, in order to be suitable for the applications in e-skin and healthcare field, future work needs to solve problems including but not limited to (a) the mechanical compliance to that of tissue and organ, (b) the antibacterial and biological safety for long-term contact with human skin and (c) the biodegradability for an implant device to monitor tissue repair progress and self-elimination away after service life. In addition to the functional performance and bioadaptability, an environmental friendship should be considered for piezoresistive sensors. The future work on e-skin calls for the green principles for designing the piezoresistive sensors, which shall consider both fabrication and material selection.

Presently, the applications of e-skin are developing explosively. The attempts based on piezoresistive design, for example, health monitoring, speech recognition, robotic device, human-machine interface, and artificial intelligence, are shaping our society toward an intelligent life. In this field, future interests can include a comprehensive biomimicking of skin functionality beyond just tactile response. This will request a piezoresistive sensor to integrate different modules and capable of detecting various basic parameters such as temperature, humidity, sweat and even metabolism. Of course, difficulties related to the integrated design of complicated circuit and the extreme precision of fabrication should be evaluated prior to the pursuit of excellent multi-responses. As discussed in this review, it is also necessary to have the feedback capability for intelligent application. Definitely, techniques that can promote an integrated connection among piezoresistive sensor, different nerves and smart equipment will advance the development of future e-skin.

## References

1. Ma Z, Li S, Wang HT, Cheng W, Li Y et al. Advanced electronic skin devices for healthcare applications. *J Mater Chem B* 7, 173–197 (2019).
2. Dolbashid AS, Mokhtar MS, Muhamad F, Ibrahim F. Potential applications of human artificial skin and electronic skin (e-skin): a review. *Bioinspir Biomim Nanobiomater* 7, 53–64 (2018).

3. Sokolov AN, Tee BCK, Bettinger CJ, Tok JBH, Bao ZN. Chemical and engineering approaches to enable organic field-effect transistors for electronic skin applications. *Acc Chem Res* **45**, 361–371 (2012).
4. Zhang L, Pan J, Zhang Z, Wu H, Yao N et al. Ultrasensitive skin-like wearable optical sensors based on glass micro/nanofibers. *Opto-Electron Adv* **3**, 190022 (2020).
5. Yang JC, Mun J, Kwon SY, Park S, Bao ZN et al. Electronic skin: recent progress and future prospects for skin-attachable devices for health monitoring, robotics, and prosthetics. *Adv Mater* **31**, 1904765 (2019).
6. Qi K, He JX, Wang HB, Zhou YM, You XL et al. A highly stretchable nanofiber-based electronic skin with pressure-, strain-, and flexion-sensitive properties for health and motion monitoring. *ACS Appl Mater Interfaces* **9**, 42951–42960 (2017).
7. dos Santos A, Pinela N, Alves P, Santos R, Fortunato E et al. Piezoresistive e-skin sensors produced with laser engraved molds. *Adv Electron Mater* **4**, 1800182 (2018).
8. Wang LL, Wang K, Lou Z, Jiang K, Shen GZ. Plant-based modular building blocks for “green” electronic skins. *Adv Funct Mater* **28**, 1804510 (2018).
9. Liu CY, Huang NG, Xu F, Tong JD, Chen ZW et al. 3D printing technologies for flexible tactile sensors toward wearable electronics and electronic skin. *Polymers* **10**, 629 (2018).
10. Hammock ML, Chortos A, Tee BCK, Tok JBH, Bao ZN. 25th anniversary article: the evolution of electronic skin (e-skin): a brief history, design considerations, and recent progress. *Adv Mater* **25**, 5997–6038 (2013).
11. Jiang FK, Tai YC, Walsh K, Tsao T, Lee GB et al. A flexible MEMS technology and its first application to shear stress sensor skin. In *IEEE the Tenth Annual International Workshop on Micro Electro Mechanical Systems. An Investigation of Micro Structures, Sensors, Actuators, Machines and Robots* 465–470 (IEEE, 1997); <http://doi.org/10.1109/MEMSYS.1997.581894>.
12. Wang C, Hwang D, Yu ZB, Takei K, Park J et al. User-interactive electronic skin for instantaneous pressure visualization. *Nat Mater* **12**, 899–904 (2013).
13. Tee BCK, Chortos A, Berndt A, Nguyen AK, Tom A et al. A skin-inspired organic digital mechanoreceptor. *Science* **350**, 313–316 (2015).
14. Someya T, Sekitani T, Iba S, Kato Y, Kawaguchi H et al. A large-area, flexible pressure sensor matrix with organic field-effect transistors for artificial skin applications. *Proc Natl Acad Sci USA* **101**, 9966–9970 (2004).
15. Su B, Gong S, Ma Z, Yap LW, Cheng WL. Mimosa-inspired design of a flexible pressure sensor with touch sensitivity. *Small* **11**, 1886–1891 (2015).
16. Kang D, Pikhitsa PV, Choi YW, Lee C, Shin SS et al. Ultrasensitive mechanical crack-based sensor inspired by the spider sensory system. *Nature* **516**, 222–226 (2014).
17. Zou ZN, Zhu CP, Li Y, Lei XF, Zhang W et al. Rehealable, fully recyclable, and malleable electronic skin enabled by dynamic covalent thermoset nanocomposite. *Sci Adv* **4**, eaaq0508 (2018).
18. Lou Z, Chen S, Wang LL, Jiang K, Shen GZ. An ultra-sensitive and rapid response speed graphene pressure sensors for electronic skin and health monitoring. *Nano Energy* **23**, 7–14 (2016).
19. Park J, Kim M, Lee Y, Lee HS, Ko H. Fingertip skin-inspired microstructured ferroelectric skins discriminate static/dynamic pressure and temperature stimuli. *Sci Adv* **1**, e1500661 (2015).
20. Wang SH, Xu J, Wang WC, Wang GJN, Rastak R et al. Skin electronics from scalable fabrication of an intrinsically stretchable transistor array. *Nature* **555**, 83–88 (2018).
21. Someya T, Kato Y, Sekitani T, Iba S, Noguchi Y et al. Conformable, flexible, large-area networks of pressure and thermal sensors with organic transistor active matrixes. *Proc Natl Acad Sci USA* **102**, 12321–12325 (2005).
22. Benight SJ, Wang C, Tok JBH, Bao ZN. Stretchable and self-healing polymers and devices for electronic skin. *Prog Polym Sci* **38**, 1961–1977 (2013).
23. Chortos A, Liu J, Bao ZN. Pursuing prosthetic electronic skin. *Nat Mater* **15**, 937–950 (2016).
24. Miao P, Wang J, Zhang CC, Sun MY, Cheng SS et al. Graphene nanostructure-based tactile sensors for electronic skin applications. *Nano-Micro Lett* **11**, 71 (2019).
25. Chortos A, Bao ZN. Skin-inspired electronic devices. *Mater Today* **17**, 321–331 (2014).
26. Chen D, Pei QB. Electronic muscles and skins: a review of soft sensors and actuators. *Chem Rev* **117**, 11239–11268 (2017).
27. Li T, Luo H, Qin L, Wang XW, Xiong ZP et al. Flexible capacitive tactile sensor based on micropatterned dielectric layer. *Small* **12**, 5042–5048 (2016).
28. Lu XZ, Yang JY, Qi L, Bao WM, Zhao L et al. High sensitivity flexible electronic skin based on graphene film. *Sensors* **19**, 794 (2019).
29. Jason NN, Ho MD, Cheng WL. Resistive electronic skin. *J Mater Chem C* **5**, 5845–5866 (2017).
30. Kwon SN, Kim SW, Kim IG, Hong YK, Na SI. Direct 3D printing of graphene nanoplatelet/silver nanoparticle-based nanocomposites for multiaxial piezoresistive sensor applications. *Adv Mater Technol* **4**, 1800500 (2019).
31. Esposito D, Andreozzi E, Fratini A, Gargiulo GD, Savino S et al. A piezoresistive sensor to measure muscle contraction and mechanomyography. *Sensors* **18**, 2553 (2018).
32. Sengupta D, Pei YT, Kottapalli AGP. Ultralightweight and 3D squeezable graphene-polydimethylsiloxane composite foams as piezoresistive sensors. *ACS Appl Mater Interfaces* **11**, 35201–35211 (2019).
33. Li X, Li Y, Li X, Song D, Min P et al. Highly sensitive, reliable and flexible piezoresistive pressure sensors featuring polyurethane sponge coated with MXene sheets. *J Colloid Interface Sci* **542**, 54–62 (2019).
34. Wu YC, Karakurt I, Beker L, Kubota Y, Xu RX et al. Piezoresistive stretchable strain sensors with human machine interface demonstrations. *Sens Actuators A:Phys* **279**, 46–52 (2018).
35. Wu P, Xiao A, Zhao YN, Chen FX, Ke MF et al. An implantable and versatile piezoresistive sensor for the monitoring of human-machine interface interactions and the dynamical process of nerve repair. *Nanoscale* **11**, 21103–21118 (2019).
36. Azhari S, Termeh Yousefi A, Tanaka H, Khajeh A, Kuredemus N et al. Fabrication of piezoresistive based pressure sensor via purified and functionalized CNTs/PDMS nanocomposite: toward development of haptic sensors. *Sens Actuators A:Phys* **266**, 158–165 (2017).
37. Phan HP, Dao DV, Nakamura K, Dimitrijević S, Nguyen NT. The piezoresistive effect of SiC for MEMS sensors at high temperatures: a review. *J Microelectromech Syst* **24**, 1663–1677

- (2015).
38. Ferreira A, Silva JP, Rodrigues R, Martin N, Lanceros-Méndez S et al. High performance piezoresistive response of nanostructured ZnO/Ag thin films for pressure sensing applications. *Thin Solid Films* **691**, 137587 (2019).
  39. Rowe ACH. Piezoresistance in silicon and its nanostructures. *J Mater Res* **29**, 731–744 (2014).
  40. Smith CS. Piezoresistance effect in germanium and silicon. *Phys Rev* **94**, 42–49 (1954).
  41. Barlian AA, Park WT, Mallon JR, Rastegar AJ, Pruitt BL. Review: semiconductor piezoresistance for microsystems. *Proc IEEE* **97**, 513–552 (2009).
  42. Stassi S, Cauda V, Canavese G, Pirri CF. Flexible tactile sensing based on piezoresistive composites: a review. *Sensors* **14**, 5296–5332 (2014).
  43. Obitayo W, Liu T. A review: carbon nanotube-based piezoresistive strain sensors. *J Sens* **2012**, 652438 (2012).
  44. Quirós-Solano WF, Gaio N, Silvestri C, Pandraud G, Dekker R et al. Metal and polymeric strain gauges for Si-based, monolithically fabricated organs-on-chips. *Micromachines* **10**, 536 (2019).
  45. Yousef H, Boukallel M, Althoefer K. Tactile sensing for dexterous in-hand manipulation in robotics—a review. *Sens Actuators A:Phys* **167**, 171–187 (2011).
  46. Peng Y, Liu HZ, Li TQ, Zhang JY. Hybrid metallic foam with superior elasticity, high electrical conductivity, and pressure sensitivity. *ACS Appl Mater Interfaces* **12**, 6489–6495 (2020).
  47. Fiorillo AS, Critello CD, Pullano SA. Theory, technology and applications of piezoresistive sensors: a review. *Sens Actuators A:Phys* **281**, 156–175 (2018).
  48. Taherian R. Development of an equation to model electrical conductivity of polymer-based carbon nanocomposites. *ECS J Solid State Sci Technol* **3**, M26–M38 (2014).
  49. Wang LH, Cheng LH. Piezoresistive effect of a carbon nanotube silicone-matrix composite. *Carbon* **71**, 319–331 (2014).
  50. Shajari S, Mahmoodi M, Rajabian M, Karan K, Sundararaj U et al. Highly sensitive and stretchable carbon nanotube/fluoroelastomer nanocomposite with a double-percolated network for wearable electronics. *Adv Electron Mater* **6**, 1901067 (2020).
  51. Wang XD, Wang JC, Biswas S, Kim H, Nam I. Mechanical, electrical, and piezoresistive sensing characteristics of epoxy-based composites incorporating hybridized networks of carbon nanotubes, graphene, carbon nanofibers, or graphite nanoplatelets. *Sensors* **20**, 2094 (2020).
  52. Ding YC, Yang J, Tolle CR, Zhu ZT. Flexible and compressible PEDOT: PSS@melamine conductive sponge prepared via one-step dip coating as piezoresistive pressure sensor for human motion detection. *ACS Appl Mater Interfaces* **10**, 16077–16086 (2018).
  53. Li F, Shen T, Wang C, Zhang YP, Qi JJ et al. Recent advances in strain-induced piezoelectric and piezoresistive effect-engineered 2D semiconductors for adaptive electronics and optoelectronics. *Nano-Micro Lett* **12**, 106 (2020).
  54. Kumar SS, Pant BD. Design principles and considerations for the 'ideal' silicon piezoresistive pressure sensor: a focused review. *Microsyst Technol* **20**, 1213–1247 (2014).
  55. Wee KW, Kang GY, Park J, Kang JY, Yoon DS et al. Novel electrical detection of label-free disease marker proteins using piezoresistive self-sensing micro-cantilevers. *Biosens Bioelectron* **20**, 1932–1938 (2005).
  56. Zhang SS, Yen SC, Xiang ZL, Liao LD, Kwong DL et al. Development of silicon probe with acute study on *in vivo* neural recording and implantation behavior monitored by integrated Si-nanowire strain sensors. *J Microelectromech Syst* **24**, 1303–1313 (2015).
  57. Marsi N, Majlis BY, Hamzah AA, Mohd-Yasin F. Development of high temperature resistant of 500 °C employing silicon carbide (3C-SiC) based MEMS pressure sensor. *Microsyst Technol* **21**, 319–330 (2015).
  58. Poncé S, Margine ER, Giustino F. Towards predictive many-body calculations of phonon-limited carrier mobilities in semiconductors. *Phys Rev B* **97**, 121201 (2018).
  59. Won SM, Wang HL, Kim BH, Lee K, Jang H et al. Multimodal sensing with a three-dimensional piezoresistive structure. *ACS Nano* **13**, 10972–10979 (2019).
  60. Yang QS, Lee S, Xue YG, Yan Y, Liu TL et al. Materials, mechanics designs, and bioresorbable multisensor platforms for pressure monitoring in the intracranial space. *Adv Funct Mater* **30**, 1910718 (2020).
  61. Okojie RS, Lukco D, Nguyen V, Savrun E. 4H-SiC Piezoresistive pressure sensors at 800 °C with observed sensitivity recovery. *IEEE Electron Device Lett* **36**, 174–176 (2015).
  62. Nguyen TK, Phan HP, Dinh T, Dowling KM, Faisal AR et al. Highly sensitive 4H-SiC pressure sensor at cryogenic and elevated temperatures. *Mater Des* **156**, 441–445 (2018).
  63. Jayasree A, Kottappally Thankappan S, Ramachandran R, Sundaram MN, Chen CH et al. Bioengineered braided micro-nano (multiscale) fibrous scaffolds for tendon reconstruction. *ACS Biomater Sci Eng* **5**, 1476–1486 (2019).
  64. Park M, Kim MS, Park YK, Ahn JH. Si membrane based tactile sensor with active matrix circuitry for artificial skin applications. *Appl Phys Lett* **106**, 043502 (2015).
  65. Gao Y, Li Q, Wu RY, Sha J, Lu YF et al. Laser direct writing of ultrahigh sensitive SiC-based strain sensor arrays on elastomer toward electronic skins. *Adv Funct Mater* **29**, 1806786 (2019).
  66. Bi P, Liu XW, Yang Y, Wang ZY, Shi J et al. Silver-nanoparticle-modified polyimide for multiple artificial skin-sensing applications. *Adv Mater Technol* **4**, 1900426 (2019).
  67. Dong DD, Ma JZ, Ma ZL, Chen YM, Zhang HM et al. Flexible and lightweight microcellular rGO@pebax composites with synergistic 3D conductive channels and microcracks for piezoresistive sensors. *Compos A:Appl Sci Manuf* **123**, 222–231 (2019).
  68. Ma YN, Yue Y, Zhang H, Cheng F, Zhao WQ et al. 3D synergistic MXene/reduced graphene oxide aerogel for a piezoresistive sensor. *ACS Nano* **12**, 3209–3216 (2018).
  69. Oh J, Kim JO, Kim Y, Choi HB, Yang JC et al. Highly uniform and low hysteresis piezoresistive pressure sensors based on chemical grafting of polypyrrole on elastomer template with uniform pore size. *Small* **15**, 1901744 (2019).
  70. Li S, Zhang Y, Wang YL, Xia KL, Yin Z et al. Physical sensors for skin-inspired electronics. *InfoMat* **2**, 184–211 (2020).
  71. Zhang CY, Zhou W, Geng D, Bai C, Li WD et al. Laser direct writing and characterizations of flexible piezoresistive sensors with microstructures. *Opto-Electron Adv* **4**, 200061 (2021).
  72. El Zein A, Huppe C, Cochrane C. Development of a flexible strain sensor based on PEDOT: PSS for thin film structures. *Sensors* **17**, 1337 (2017).

73. Sezen-Edmonds M, Yeh YW, Yao N, Loo YL. Humidity and strain rate determine the extent of phase shift in the piezoresistive response of PEDOT: PSS. *ACS Appl Mater Interfaces* **11**, 16888–16895 (2019).
74. Fan X, Wang NX, Yan F, Wang JZ, Song W et al. A transfer-printed, stretchable, and reliable strain sensor using PEDOT: PSS/Ag NW hybrid films embedded into elastomers. *Adv Mater Technol* **3**, 1800030 (2018).
75. Li DD, Lai WY, Zhang YZ, Huang W. Printable transparent conductive films for flexible electronics. *Adv Mater* **30**, 1704738 (2018).
76. Zhang SD, Liu H, Yang SY, Shi XZ, Zhang DB et al. Ultrasensitive and highly compressible piezoresistive sensor based on polyurethane sponge coated with a cracked cellulose nanofibril/silver nanowire layer. *ACS Appl Mater Interfaces* **11**, 10922–10932 (2019).
77. Herren B, Saha MC, Liu YT. Carbon nanotube-based piezoresistive sensors fabricated by microwave irradiation. *Adv Eng Mater* **22**, 1901068 (2020).
78. Nguyen NA, Meek KM, Bowland CC, Barnes SH, Naskar AK. An acrylonitrile–butadiene–lignin renewable skin with programmable and switchable electrical conductivity for stress/strain-sensing applications. *Macromolecules* **51**, 115–127 (2018).
79. Ruschau GR, Yoshikawa S, Newnham RE. Resistivities of conductive composites. *J Appl Phys* **72**, 953–959 (1992).
80. Wang S, Chen GR, Niu SY, Chen KF, Gan T et al. Magnetic-assisted transparent and flexible percolative composite for highly sensitive piezoresistive sensor via hot embossing technology. *ACS Appl Mater Interfaces* **11**, 48331–48340 (2019).
81. Zhang XH, Sheng NN, Wang LN, Tan YQ, Liu CZ et al. Supramolecular nanofibrillar hydrogels as highly stretchable, elastic and sensitive ionic sensors. *Mater Horiz* **6**, 326–333 (2019).
82. Luo NQ, Huang Y, Liu J, Chen SC, Wong CP et al. Hollow-structured graphene-silicone-composite-based piezoresistive sensors: decoupled property tuning and bending reliability. *Adv Mater* **29**, 1702675 (2017).
83. Xu MX, Li F, Zhang ZY, Shen T, Qi JJ. Piezoresistive sensors based on rGO 3D microarchitecture: coupled properties tuning in local/integral deformation. *Adv Electron Mater* **5**, 1800461 (2019).
84. Khalili N, Shen X, Naguib HE. An interlocked flexible piezoresistive sensor with 3D micropyramidal structures for electronic skin applications. *Soft Matter* **14**, 6912–6920 (2018).
85. Ji B, Zhou Q, Wu J, Gao Y, Wen W et al. Synergistic Optimization toward the Sensitivity and Linearity of Flexible Pressure Sensor via Double Conductive Layer and Porous Microdome Array. *ACS Appl Mater Interfaces* **12**, 31021–31035 (2020).
86. Ji B, Mao YY, Zhou Q, Zhou JH, Chen G et al. Facile preparation of hybrid structure based on mesodome and micropillar arrays as flexible electronic skin with tunable sensitivity and detection range. *ACS Appl Mater Interfaces* **11**, 28060–28071 (2019).
87. Zhang P, Chen YC, Li YX, Zhao Y, Wang W et al. Flexible piezoresistive sensor with the microarray structure based on self-assembly of multi-walled carbon nanotubes. *Sensors* **19**, 4985 (2019).
88. Pan LJ, Chortos A, Yu GH, Wang YQ, Isaacson S et al. An ultra-sensitive resistive pressure sensor based on hollow-sphere microstructure induced elasticity in conducting polymer film. *Nat Commun* **5**, 3002 (2014).
89. Bae GY, Pak SW, Kim D, Lee G, Kim DH et al. Linearly and highly pressure-sensitive electronic skin based on a bioinspired hierarchical structural array. *Adv Mater* **28**, 5300–5306 (2016).
90. Huang Y, Fan XY, Chen SC, Zhao N. Emerging technologies of flexible pressure sensors: materials, modeling, devices, and manufacturing. *Adv Funct Mater* **29**, 1808509 (2019).
91. Huang ZL, Gao M, Yan ZC, Pan TS, Khan SA et al. Pyramid microstructure with single walled carbon nanotubes for flexible and transparent micro-pressure sensor with ultra-high sensitivity. *Sens Actuators A:Phys* **266**, 345–351 (2017).
92. Gao Y, Lu C, Yu GH, Sha J, Tan JP et al. Laser micro-structured pressure sensor with modulated sensitivity for electronic skins. *Nanotechnology* **30**, 325502 (2019).
93. dos Santos A, Pinela N, Alves P, Santos R, Farinha R et al. E-skin bimodal sensors for robotics and prosthesis using PDMS molds engraved by laser. *Sensors* **19**, 899 (2019).
94. Park J, Kim J, Hong J, Lee H, Lee Y et al. Tailoring force sensitivity and selectivity by microstructure engineering of multidirectional electronic skins. *NPG Asia Mater* **10**, 163–176 (2018).
95. Wang ZR, Wang S, Zeng JF, Ren XC, Chee AJY et al. High sensitivity, wearable, piezoresistive pressure sensors based on irregular microhump structures and its applications in body motion sensing. *Small* **12**, 3827–3836 (2016).
96. Jia WD, Zhang Q, Cheng YQ, Zhao D, Liu Y et al. Flexible and highly sensitive piezoresistive pressure sensor with sandpaper as a mold. *Nano* **14**, 1950081 (2019).
97. Wang LL, Chen D, Jiang K, Shen GZ. New insights and perspectives into biological materials for flexible electronics. *Chem Soc Rev* **46**, 6764–6815 (2017).
98. Shi JD, Wang L, Dai ZH, Zhao LY, Du MD et al. Multiscale hierarchical design of a flexible piezoresistive pressure sensor with high sensitivity and wide linearity range. *Small* **14**, 1800819 (2018).
99. Wei Y, Chen S, Lin Y, Yang ZM, Liu L. Cu–Ag core–shell nanowires for electronic skin with a petal molded microstructure. *J Mater Chem C* **3**, 9594–9602 (2015).
100. Jian MQ, Xia KL, Wang Q, Yin Z, Wang HM et al. Flexible and highly sensitive pressure sensors based on bionic hierarchical structures. *Adv Funct Mater* **27**, 1606066 (2017).
101. Jang HH, Park JS, Choi B. Flexible piezoresistive pulse sensor using biomimetic PDMS mold replicated negatively from shark skin and PEDOT: PSS thin film. *Sens Actuators A:Phys* **286**, 107–114 (2019).
102. Chen ZM, Liu XH, Wang SM, Zhang XX, Luo HS. A bioinspired multilayer assembled microcrack architecture nanocomposite for highly sensitive strain sensing. *Compos Sci Technol* **164**, 51–58 (2018).
103. Nie P, Wang RR, Xu XJ, Cheng Y, Wang X et al. High-performance piezoresistive electronic skin with bionic hierarchical microstructure and microcracks. *ACS Appl Mater Interfaces* **9**, 14911–14919 (2017).
104. Yang TT, Li XM, Jiang X, Lin SY, Lao JC et al. Structural engineering of gold thin films with channel cracks for ultrasensitive strain sensing. *Mater Horiz* **3**, 248–255 (2016).
105. Shi JD, Lv SY, Wang L, Dai ZH, Yang ST et al. Crack control in biotemplated gold films for wide-range, highly sensitive strain sensing. *Adv Mater Interfaces* **6**, 1901223 (2019).
106. Zhao TT, Li TK, Chen LL, Yuan L, Li XF et al. Highly sensitive

- flexible piezoresistive pressure sensor developed using biometrically textured porous materials. *ACS Appl Mater Interfaces* **11**, 29466–29473 (2019).
107. Chen M, Li K, Cheng GM, He K, Li WW et al. Touchpoint-tailored ultrasensitive piezoresistive pressure sensors with a broad dynamic response range and low detection limit. *ACS Appl Mater Interfaces* **11**, 2551–2558 (2019).
  108. Sun XG, Sun JH, Zheng SK, Wang CK, Tan WS et al. A sensitive piezoresistive tactile sensor combining two microstructures. *Nanomaterials* **9**, 779 (2019).
  109. Wei Y, Chen S, Yuan X, Wang PP, Liu L. Multiscale wrinkled microstructures for piezoresistive fibers. *Adv Funct Mater* **26**, 5078–5085 (2016).
  110. Wang SC, Innocent MT, Wang QQ, Xiang HX, Tang JG et al. Kraft lignin-based piezoresistive sensors: effect of chemical structure on the microstructure of ultrathin carbon fibers. *Int J Biol Macromol* **151**, 730–739 (2020).
  111. Li J, Fang LC, Sun BH, Li XX, Kang SH. Review-recent progress in flexible and stretchable piezoresistive sensors and their applications. *J Electrochem Soc* **167**, 037561 (2020).
  112. Cao MH, Wang MQ, Li L, Qiu HW, Padhiar MA et al. Wearable rGO-Ag NW@ cotton fiber piezoresistive sensor based on the fast charge transport channel provided by Ag nanowire. *Nano Energy* **50**, 528–535 (2018).
  113. Lin XZ, Zhang T, Cao JH, Wen H, Fei T et al. Flexible piezoresistive sensors based on conducting polymer-coated fabric applied to human physiological signals monitoring. *J Bionic Eng* **17**, 55–63 (2020).
  114. Zhang L, Li HQ, Lai XJ, Gao TY, Liao XF et al. Carbonized cotton fabric-based multilayer piezoresistive pressure sensors. *Cellulose* **26**, 5001–5014 (2019).
  115. Wang Q, Jian MQ, Wang CY, Zhang YY. Carbonized silk nanofiber membrane for transparent and sensitive electronic skin. *Adv Funct Mater* **27**, 1605657 (2017).
  116. Zhao ZC, Li BT, Xu LQ, Qiao Y, Wang F et al. A sandwich-structured piezoresistive sensor with electrospun nanofiber mats as supporting, sensing, and packaging layers. *Polymers* **10**, 575 (2018).
  117. Liu WJ, Liu NS, Yue Y, Rao JY, Cheng F et al. Piezoresistive pressure sensor based on synergistical innerconnect polyvinyl alcohol nanowires/wrinkled graphene film. *Small* **14**, 1704149 (2018).
  118. Luo C, Liu NS, Zhang H, Liu WJ, Yue Y et al. A new approach for ultrahigh-performance piezoresistive sensor based on wrinkled PPy film with electrospun PVA nanowires as spacer. *Nano Energy* **41**, 527–534 (2017).
  119. Li P, Zhao LB, Jiang ZD, Yu MZ, Li Z et al. Self-powered flexible sensor based on the graphene modified P(VDF-TrFE) electrospun fibers for pressure detection. *Macromol Mater Eng* **304**, 1900504 (2019).
  120. Alam M, Lee S, Kim M, Han KS, Cao VA et al. Ultra-flexible nanofiber-based multifunctional motion sensor. *Nano Energy* **72**, 104672 (2020).
  121. Yu SL, Wang XP, Xiang HX, Zhu LP, Tebyetekerwa M et al. Superior piezoresistive strain sensing behaviors of carbon nanotubes in one-dimensional polymer fiber structure. *Carbon* **140**, 1–9 (2018).
  122. Tang ZH, Jia SH, Wang F, Bian CS, Chen YY et al. Highly stretchable core-sheath fibers via wet-spinning for wearable strain sensors. *ACS Appl Mater Interfaces* **10**, 6624–6635 (2018).
  123. Tang ZH, Jia SH, Shi S, Wang F, Li B. Coaxial carbon nanotube/polymer fibers as wearable piezoresistive sensors. *Sens Actuators A:Phys* **284**, 85–95 (2018).
  124. Charara M, Luo WY, Saha MC, Liu YT. Investigation of lightweight and flexible carbon nanofiber/poly dimethylsiloxane nanocomposite sponge for piezoresistive sensor application. *Adv Eng Mater* **21**, 1801068 (2019).
  125. Zhong Y, Tan XH, Shi TL, Huang YY, Cheng SY et al. Tunable wrinkled graphene foams for highly reliable piezoresistive sensor. *Sens Actuators A:Phys* **281**, 141–149 (2018).
  126. Zhai Y, Yu YF, Zhou KK, Yun ZG, Huang WJ et al. Flexible and wearable carbon black/thermoplastic polyurethane foam with a pinnate-veined aligned porous structure for multifunctional piezoresistive sensors. *Chem Eng J* **382**, 122985 (2020).
  127. Zhuo H, Hu YJ, Chen ZH, Peng XW, Liu LX et al. A carbon aerogel with super mechanical and sensing performances for wearable piezoresistive sensors. *J Mater Chem A* **7**, 8092–8100 (2019).
  128. Peng XW, Wu KZ, Hu YJ, Zhuo H, Chen ZH et al. A mechanically strong and sensitive CNT/rGO–CNF carbon aerogel for piezoresistive sensors. *J Mater Chem A* **6**, 23550–23559 (2018).
  129. Yang CX, Liu WJ, Liu NS, Su J, Li LY et al. Graphene aerogel broken to fragments for a piezoresistive pressure sensor with a higher sensitivity. *ACS Appl Mater Interfaces* **11**, 33165–33172 (2019).
  130. Ma ZL, Wei AJ, Ma JZ, Shao L, Jiang HE et al. Lightweight, compressible and electrically conductive polyurethane sponges coated with synergistic multiwalled carbon nanotubes and graphene for piezoresistive sensors. *Nanoscale* **10**, 7116–7126 (2018).
  131. Pang Y, Tian H, Tao LQ, Li YX, Wang XF et al. Flexible, highly sensitive, and wearable pressure and strain sensors with graphene porous network structure. *ACS Appl Mater Interfaces* **8**, 26458–26462 (2016).
  132. Zheng SD, Wu XT, Huang YH, Xu ZW, Yang W et al. Highly sensitive and multifunctional piezoresistive sensor based on polyaniline foam for wearable human-activity monitoring. *Compos A:Appl Sci Manuf* **121**, 510–516 (2019).
  133. Zhai W, Xia QJ, Zhou KK, Yue XY, Ren MN et al. Multifunctional flexible carbon black/polydimethylsiloxane piezoresistive sensor with ultrahigh linear range, excellent durability and oil/water separation capability. *Chem Eng J* **372**, 373–382 (2019).
  134. Wu YH, Liu HZ, Chen S, Dong XC, Wang PP et al. Channel crack-designed gold@PU sponge for highly elastic piezoresistive sensor with excellent detectability. *ACS Appl Mater Interfaces* **9**, 20098–20105 (2017).
  135. Wang T, Li JH, Zhang Y, Liu F, Zhang B et al. Highly ordered 3D porous graphene sponge for wearable piezoresistive pressure sensor applications. *Chem Eur J* **25**, 6378–6384 (2019).
  136. Huang WJ, Dai K, Zhai Y, Liu H, Zhan PF et al. Flexible and lightweight pressure sensor based on carbon nanotube/thermoplastic polyurethane-aligned conductive foam with superior compressibility and stability. *ACS Appl Mater Interfaces* **9**, 42266–42277 (2017).
  137. Abshirini M, Charara M, Liu YT, Saha M, Altan MC. 3D printing of highly stretchable strain sensors based on carbon nanotube nanocomposites. *Adv Eng Mater* **20**, 1800425 (2018).

138. Crump MR, Gong AT, Chai D, Bidinger SL, Pavinatto FJ et al. Monolithic 3D printing of embeddable and highly stretchable strain sensors using conductive ionogels. *Nanotechnology* **30**, 364002 (2019).
139. Kelleher SM, Habimana O, Lawler J, Reilly BO, Daniels S et al. Cicada wing surface topography: an investigation into the bactericidal properties of nanostructural features. *ACS Appl Mater Interfaces* **8**, 14966–14974 (2016).
140. Guo SZ, Qiu KY, Meng FB, Park SH, McAlpine MC. 3D printed stretchable tactile sensors. *Adv Mater* **29**, 1701218 (2017).
141. Goh GL, Agarwala S, Yeong WY. Directed and on-demand alignment of carbon nanotube: a review toward 3D printing of electronics. *Adv Mater Interfaces* **6**, 1801318 (2019).
142. Nadgorny M, Ameli A. Functional polymers and nanocomposites for 3D printing of smart structures and devices. *ACS Appl Mater Interfaces* **10**, 17489–17507 (2018).
143. Davoodi E, Fayazfar H, Liravi F, Jabari E, Toyserkani E. Drop-on-demand high-speed 3D printing of flexible milled carbon fiber/silicone composite sensors for wearable biomonitors devices. *Addit Manuf* **32**, 101016 (2020).
144. Wang HH, Yang HM, Zhang S, Zhang L, Li JS et al. 3D-printed flexible tactile sensor mimicking the texture and sensitivity of human skin. *Adv Mater Technol* **4**, 1900147 (2019).
145. Tang ZH, Jia SH, Zhou CH, Li B. 3D printing of highly sensitive and large-measurement-range flexible pressure sensors with a positive piezoresistive effect. *ACS Appl Mater Interfaces* **12**, 28669–28680 (2020).
146. Wei PQ, Yang X, Cao ZM, Guo XL, Jiang HL et al. Flexible and stretchable electronic skin with high durability and shock resistance via embedded 3D printing technology for human activity monitoring and personal healthcare. *Adv Mater Technol* **4**, 1900315 (2019).
147. Wang ZY, Guan X, Huang HY, Wang HF, Lin WE et al. Full 3D printing of stretchable piezoresistive sensor with hierarchical porosity and multimodulus architecture. *Adv Funct Mater* **29**, 1807569 (2019).
148. Kim JY, Ji S, Jung S, Ryu BH, Kim HS et al. 3D printable composite dough for stretchable, ultrasensitive and body-patchable strain sensors. *Nanoscale* **9**, 11035–11046 (2017).
149. Huang K, Dong SM, Yang JS, Yan JY, Xue YD et al. Three-dimensional printing of a tunable graphene-based elastomer for strain sensors with ultrahigh sensitivity. *Carbon* **143**, 63–72 (2019).
150. Zhou YL, Wu YZ, Asghar W, Ding J, Su XR et al. Asymmetric structure based flexible strain sensor for simultaneous detection of various human joint motions. *ACS Appl Electron Mater* **1**, 1866–1872 (2019).
151. Han T, Kundu S, Nag A, Xu YZ. 3D printed sensors for biomedical applications: a review. *Sensors* **19**, 1706 (2019).
152. Gong TX, Zhang H, Huang W, Mao LN, Ke YZ et al. Highly responsive flexible strain sensor using polystyrene nanoparticle doped reduced graphene oxide for human health monitoring. *Carbon* **140**, 286–295 (2018).
153. Guan X, Wang ZY, Zhao WY, Huang HY, Wang SP et al. Flexible piezoresistive sensors with wide-range pressure measurements based on a graded nest-like architecture. *ACS Appl Mater Interfaces* **12**, 26137–26144 (2020).
154. Ramírez J, Rodríguez D, Urbina AD, Cardenas AM, Lipomi DJ. Combining high sensitivity and dynamic range: wearable thin-film composite strain sensors of graphene, ultrathin palladium, and PEDOT: PSS. *ACS Appl Nano Mater* **2**, 2222–2229 (2019).
155. Tewari A, Gandla S, Bohm S, McNeill CR, Gupta D. Rapid dip-dry MWNT-rGO ink wrapped polyester elastic band (PEB) for piezoresistive strain sensor applications. *Appl Phys Lett* **113**, 084101 (2018).
156. Ruth SRA, Beker L, Tran H, Feig VR, Matsuhisa N et al. Rational design of capacitive pressure sensors based on pyramidal microstructures for specialized monitoring of biosignals. *Adv Funct Mater* **30**, 1903100 (2020).
157. Wang YP, Niu WB, Lo CY, Zhao YS, He XM et al. Interactively full-color changeable electronic fiber sensor with high stretchability and rapid response. *Adv Funct Mater* **30**, 2000356 (2020).
158. Chen XP, Luo F, Yuan M, Xie DL, Shen L et al. A dual-functional graphene-based self-alarm health-monitoring e-skin. *Adv Funct Mater* **29**, 1904706 (2019).
159. Wu Q, Qiao YC, Guo R, Naveed S, Hirtz T et al. Triode-mimicking graphene pressure sensor with positive resistance variation for physiology and motion monitoring. *ACS Nano* **14**, 10104–10114 (2020).
160. Ma YN, Liu NS, Li LY, Hu XK, Zou ZG et al. A highly flexible and sensitive piezoresistive sensor based on MXene with greatly changed interlayer distances. *Nat Commun* **8**, 1207 (2017).
161. Zhang L, Li HQ, Lai XJ, Gao TY, Yang J et al. Thiolated graphene@polyester fabric-based multilayer piezoresistive pressure sensors for detecting human motion. *ACS Appl Mater Interfaces* **10**, 41784–41792 (2018).
162. Zhang Y, Chang TH, Jing L, Li KR, Yang HT et al. Heterogeneous, 3D architecture of 2D titanium carbide (MXene) for microdroplet manipulation and voice recognition. *ACS Appl Mater Interfaces* **12**, 8392–8402 (2020).
163. Yu R, Xia TC, Wu B, Yuan J, Ma LJ et al. Highly sensitive flexible piezoresistive sensor with 3D conductive network. *ACS Appl Mater Interfaces* **12**, 35291–35299 (2020).
164. Deng CH, Gao PX, Lan LF, He PH, Zhao X et al. Ultrasensitive and highly stretchable multifunctional strain sensors with timbre-recognition ability based on vertical graphene. *Adv Funct Mater* **29**, 1907151 (2019).
165. Dinh Le TS, An JN, Huang Y, Vo Q, Boonruangkan J et al. Ultrasensitive anti-interference voice recognition by bio-inspired skin-attachable self-cleaning acoustic sensors. *ACS Nano* **13**, 13293–13303 (2019).
166. Gao YY, Yan C, Huang HC, Yang T, Tian G et al. Microchannel-confined MXene based flexible piezoresistive multifunctional micro-force sensor. *Adv Funct Mater* **30**, 1909603 (2020).
167. Ming Y, Yang Y, Fu RP, Lu C, Zhao L et al. IPMC sensor integrated smart glove for pulse diagnosis, braille recognition, and human-computer interaction. *Adv Mater Technol* **3**, 1800257 (2018).
168. Dong WT, Yang L, Fortino G. Stretchable human machine interface based on smart glove embedded with PDMS-CB strain sensors. *IEEE Sens J* **20**, 8073–8081 (2020).
169. Liu SB, Wu X, Zhang DD, Guo CW, Wang P et al. Ultrafast dynamic pressure sensors based on graphene hybrid structure. *ACS Appl Mater Interfaces* **9**, 24148–24154 (2017).
170. Sencadas V, Tawk C, Alici G. Highly sensitive soft foam sensors to empower robotic systems. *Adv Mater Technol* **4**, 1900423 (2019).

171. Zhong WB, Jiang HQ, Jia KY, Ding XC, Yadav A et al. Breathable and large curved area perceptible flexible piezoresistive sensors fabricated with conductive nanofiber assemblies. *ACS Appl Mater Interfaces* **12**, 37764–37773 (2020).
172. Liang JL, Wu JH, Huang HL, Xu WF, Li B et al. Soft sensitive skin for safety control of a nursing robot using proximity and tactile sensors. *IEEE Sens J* **20**, 3822–3830 (2020).
173. Chang TH, Tian Y, Li CS, Gu XY, Li KR et al. Stretchable graphene pressure sensors with Shar-Pei-like hierarchical wrinkles for collision-aware surgical robotics. *ACS Appl Mater Interfaces* **11**, 10226–10236 (2019).
174. Ferreira A, Correia V, Mendes E, Lopes C, Vaz JFV et al. Piezoresistive polymer-based materials for real-time assessment of the stump/socket interface pressure in lower limb amputees. *IEEE Sens J* **17**, 2182–2190 (2017).
175. Kim Y, Chortos A, Xu WT, Liu YX, Oh JY et al. A bioinspired flexible organic artificial afferent nerve. *Science* **360**, 998–1003 (2018).
176. Wang Y, Wu HT, Xu L, Zhang HN, Yang Y et al. Hierarchically patterned self-powered sensors for multifunctional tactile sensing. *Sci Adv* **6**, eabb9083 (2020).
177. Lee K, Ni XY, Lee JY, Arafa H, Pe DJ et al. Mechano-acoustic sensing of physiological processes and body motions via a soft wireless device placed at the suprasternal notch. *Nat Biomed Eng* **4**, 148–158 (2020).
178. Yang HT, Xiao X, Li ZP, Li KR, Cheng N et al. Wireless  $\text{Ti}_3\text{C}_2\text{T}_x$  MXene strain sensor with ultrahigh sensitivity and designated working windows for soft exoskeletons. *ACS Nano* **14**, 11860–11875 (2020).

## Acknowledgements

This research was supported by the Hunan Provincial Technology Innovation Platform and Talent Program (2017XK2047), the Outstanding Youth Scientist Foundation of Hunan Province (2020JJ2001), and Fundamental Research Funds for the Central Universities of P R China (531107050927). Dr Z Wang received financial support from Hunan University for the Yuelu Young Scholars (JY-Q/008/2016).

## Author contributions

Z. Y. Wang conceived the original ideas of this manuscript. All authors participated in the literature review, discussion and writing of the manuscript. F. Zhong and Z. Y. Wang executed the figure drawings. Z. Y. Wang directed the work.

## Competing interests

The authors declare no competing financial interests.